minerals

MDPI

Article

Mining Exploration, Raw Materials and Production Technologies of Mortars in the Different Civilization Periods in Menorca Island (Spain)

Stefano Columbu [1,*], Anna Depalmas [2], Giovanni Brodu [1], Gianni Gallello [3] and Dario Fancello [1]

[1] Department of Chemical and Geological Sciences, Cagliari University, Cittadella Universitaria of Monserrato, 09042 Cagliari, Italy; brodu97@gmail.com (G.B.); dario.fancello@unica.it (D.F.)
[2] Department of Humanities and Social Sciences, Sassari University, Via Roma 51, 07100 Sassari, Italy; depalmas@uniss.it
[3] Department of Prehistory, Archaeology and Ancient History, Valencia University, Av. Blasco Ibáñez 28, 46010 Valencia, Spain; gianni.gallello@uv.es
* Correspondence: columbus@unica.it; Tel.: +39-070-6757766

Abstract: This study deals with the mortars and subordinately rocks collected from the archaeological site of Cap de Forma, that is a "Bien de Interés Cultural" located on a cape along the southeastern coast of Menorca (Balearic Islands, Spain). Cap de Forma consists of different structures belonging to different periods and civilization phases: a fortified settlement of Talaiotic age, built in cyclopean technique and including three rooms and a rainwater cistern; a nearby necropolis of tombs (*cuevas*) excavated into the cliff; a more recent site occupancy testified by plastering of the cistern; a *house-fort* (*pecheña casa-quartel*), a lookout point of the 17th–18th century. Compositional features and mineralogy of mortars and rocks were investigated by optical microscopy and X-ray diffraction. Physical properties (density, porosity, water saturation and water saturation coefficients and mechanical strength) were also determined. This work is aimed at characterizing these archaeologic remains to understand the building technique, the choice of raw materials and possibly their provenance, taking into account the age and civilization they belong to. Results indicate that cocciopesto-rich mortars were used in the cistern watertight and other ancient structures linking from a Roman age. The cocciopesto seems to derive from local pottery even if some evidence would suggest the contrary, whereas the source of the binder is definitely the local Mg-rich limestone. The *house-fort* was plastered with gypsum-based mortars in the 17th–18th century. The most likely source of raw gypsum was the island of Mallorca where some quarries were opened in the same period. Mechanical and physical tests reveal a strong state of decay that requires conservation actions. This work sheds light on a poorly studied monument, better constraining the different phases of its occupation. Some interesting questions, such as the cocciopesto provenance, are still open.

Keywords: Menorca Island; Cap de Forma; Talaiotic culture; Roman cocciopesto mortar; air lime mortar; gypsum mortar; raw materials supply; chemical-physical degradation; ancient quarry

Citation: Columbu, S.; Depalmas, A.; Brodu, G.; Gallello, G.; Fancello, D. Mining Exploration, Raw Materials and Production Technologies of Mortars in the Different Civilization Periods in Menorca Island (Spain). *Minerals* **2022**, *12*, 218. https://doi.org/10.3390/min12020218

Academic Editor: Adrián Durán Benito

Received: 24 December 2021
Accepted: 4 February 2022
Published: 8 February 2022

1. Introduction

Since ancient times, mineral prospecting has been a very important activity allowing the populations to recognize the georesources offered by their territories, to be used as construction materials and/or for the artefact production. Several studies, during the last sixty years, have been addressed to the determination of the provenance of raw materials, including stones [1–3], ceramics [4–6], glasses [7–9] and mortars [10–15].

If, on the one hand, high-value and/or rare materials were imported even from far source regions if not available on site (see for instance [16,17]), on the other hand low-value materials were mainly provided from local or nearby sources (as in the cases of

[3,18,19]). However, the supply of geomaterials from local outcrops was not always so easy, as the territory sometimes did not offer suitable materials for the work to be carried out. In the case of aggregates for mortars, the lack of high-quality materials, close to the building sites, forced the builders to make a choice between the use of the local low-quality materials (more economic) or the supply from a wider area (more functional) [19]. The aggregates' provision implied the quarrying from rocky outcrops, as well as from sedimentary deposits located in various environment-depositional contexts, such as river or beach deposits [19–21].

The study of ancient mortars and geomaterials represents a key moment in the study of a monument, as it allows one to understand the material supply [22–25], the construction phases of the structures [25–29], the mining prospecting activities and the technologies used in ancient times for the extraction and processing of raw materials [18,19,30], as well as the chemical-physical decay processes and conservation [31–36]. Moreover, mortars must be prepared immediately before their use and, unlike rock materials, cannot be reused in subsequent construction phases, thus they are a perfect age marker [37]. This indirectly leads to hypotheses on the construction period, on the origin of the geomaterials used as raw materials [37–39] and on commercial routes in historical times [8–41].

In the here presented research, raw materials and their processing technologies used for the mortars from the Cap de Forma archaeological site were studied. The site, also known as *Es Caparrot de Forma or Es Castellàs de Forma*, is situated on the southwest coast of Menorca Island (WGS84 coordinates: 39°50′38″N–4°10′3″E), close to Es Canutellis touristic locality (Sant Climent, Mahon Municipality), a few kilometres southwest from Menorca airport. It rests on a rocky coastal headland delimited by 30 m high sheer cliffs and is covered by the typical Mediterranean vegetation called "Maquis shrubland". Cap de Forma has been a National Monument since 1996 and later was declared a Cultural Heritage B.I.C. site (Bien de Interés Cultural) [42].

The site (Figure 1) consists of different parts belonging to different civilizations, testifying the superimposition of various cultures during its three-millennium-long history: a main rectangular monument built in cyclopean technique, a necropolis of tombs (*cuevas*) carved into the limestone, mainly placed on the cliffs, but also inland, and a rainwater cistern.

Cap de Forma archaeological complex was firstly studied in 1991 when a photographic survey was accomplished after a cleaning intervention. In the following years, several excavation campaigns were performed to bring to light the underground structures [42]. The findings of these campaigns led to some published papers, focused on the site itself, as well as extended to the importance of Talaiotic Culture in the Mediterranean context ([42–44] and references therein).

Almost all the above cited papers studied the complex from an archaeological point of view, whereas the nature of the geomaterials used in the different building phases is still poorly investigated. The general intent of this research is to contribute to today's knowledge (after [42–44]) regarding the supply and processing of geomaterials used in the structures belonging to different periods of the Cap de Forma archaeological complex. In detail, the ancient mortars and stone materials found in a pit within the cyclopean technique construction area (dating back to the Talaiotic period I: 1500–1000 BC [45]), an ancient cistern for the collection of rainwater and a building called *house-fort* or *casa-quartel* (Figure 2a,b) were studied. The specific objectives of the research are to define the compositional characteristics, the mixing ratio between binder and aggregate, hydraulic properties and the function and degradation of the mortars. Furthermore, through targeted laboratory analyses, the mineralogical-petrographic characteristics of the various samples and some significant physical properties (density, porosity, water saturation and water saturation coefficients, mechanical resistance) were determined.

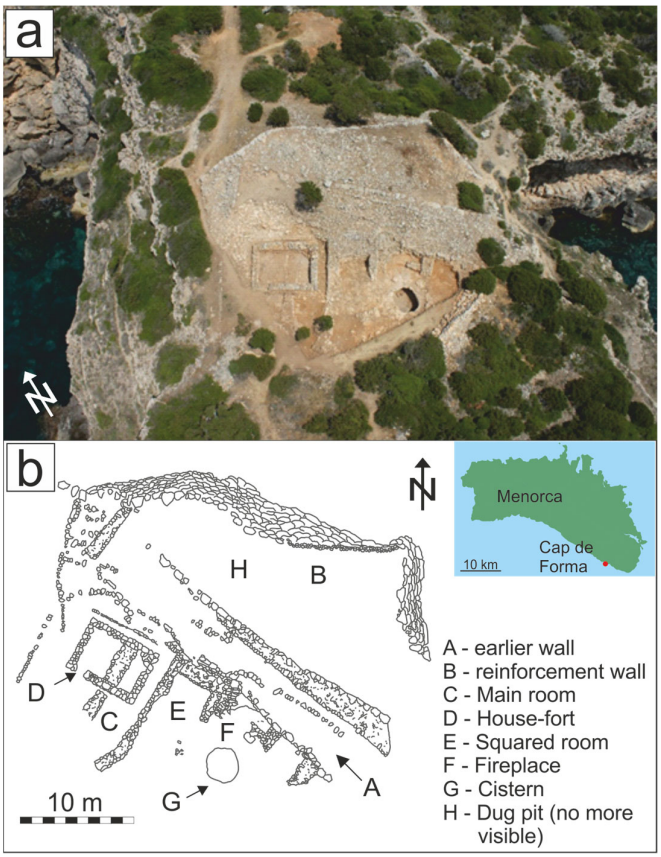

Figure 1. (**a**) Aerial view of the archaeological site of Cap de Forma (reprinted with permission from [46]. Creative commons (by-nc-nd), 2015). (**b**) Sketch map of the archaeological site indicating the most significant structures (modified after [42]).

(**a**)

(**b**)

Figure 2. (**a**) The rainwater ancient cistern excavated in the limestone in the Talaiotic time and reused in following historical period (reprinted with permission from [46]. Creative commons (by-nc-nd), 2015. (**b**) Internal view of the *house-fort* (reprinted with permission from [46]. Creative commons (by-nc-nd), 2015.

2. Site Description

As mentioned in the introduction, the Cap de Forma complex (Figure 1a) consists of different parts belonging to different civilizations and ages. The oldest part, built in cyclopean technique, is represented by a rectangular-shaped building running in NW-SE direction built to prevent foreign enemies to access the cape (Figure 1b(A)). According to Depalmas [42], this is not a Talaiot *stricto sensu* being "*different from the known archetypes of this class of monuments*" [42]. The structure was later reinforced with the construction of an external wall (Figure 1b(B)) so as, reaching the cape from inland, a huge wall, up to 4 m high and 33 m long built with roughly cut limestone ashlars, blocks the access to the cape.

The excavation campaigns have progressively brought to light the structure of the complex lying on the cape (thus protected northward by the wall) as well as those outside the wall consisting of some *cuevas*. This study is focused on the structures found in the cape, consisting of thinner walls built both parallel and perpendicular to the main wall, thus delimiting approximately rectangular rooms. From west to east the following structures are found [42]: (i) an elongated rectangular space (Figure 1b(C)), partly overlapped by the *house-fort* (Figures 1b(D) and 2b); (ii) a roughly squared room adjacent to the former (Figure 1b(E)); (iii) an irregular area that, considering the walls' remains and the traces of combustion, was probably open to the outside (southward) and used as fireplace (Figure 1b(F)); (iv) a rounded cistern used to collect rainwater in front of the fireplace (Figures 1b(G) and 2a); (v) a dug pit (Figure 1b(H)) in the upper part of the complex, north to the earlier wall.

The ancient cistern (Figure 2a), represented by a cavity (about 3 m × 3 m) found during the 2011 excavation between the central and eastern room of the Cyclopean monument, was dug in the limestone rocky substrate in the Talaiotic phase [45] and was then reused in the following periods. Its reuse is testified by several layers of mortar found at the cistern's bottom to seal the cracks in the rock, to ensure its watertightness [46].

The *house-fort* (Figure 2b), which appeared during the first archaeological excavations (1991), has been dated at the 17th to 18th century AD based on the artefacts found inside it and on documentary sources. The fort was built inside the western room of the cyclopean monument, largely using stones removed from the ancient structure and thus accelerating

its decay. The structure had an entrance door, a window (not present today) and a chimney in which several layers of ash were recognized. The internal floor is a compacted layer of soil below which the remains of a Talaiotic wall have been found.

As regards the two rooms labelled C and E in Figure 1b, neither their age nor their intended use can be precisely assessed due to the decay and to the rework of materials occurred in more recent times. However, the building technique and style and the ceramic findings led archaeologists to date back these structures to the first Talaiotic period, 1500 to 1000 BC [44,46] and to hypothesize a domestic use. Moreover, excavations are still in progress and hopefully will improve our knowledge about the site's history.

The dug pit (Figure 1b(H)), discovered in 2001, is a cavity delimited by walls and containing large lumps of lime mixed with lime-rich soil. This peculiar composition, together with the presence of walls' reinforcement of the pit suggest the use of this cavity as furnace for lime production by burning of limestone materials. Depalmas and Columbu [46] hypothesize that the pit was dug and used to produce lime for plastering the *house-fort* during its construction, thus it would date back to the 17th century.

Several artefacts and other findings, mainly ceramics but also coins and pendants, charcoal and animal bones have been found in the site and, based on the stratigraphy, have been assigned to the different occupation periods; further details can be found in [42–46] and references therein.

3. Geological Setting of Menorca Island

Menorca is the easternmost of the Balearic Islands, which are the emerged part of a raised platform called Balearic Promontory, located in the western Mediterranean and surrounded by the Valencia channel, the Algerian basin and the Ligurian basin [47,48]. The basins were generated during the late Oligocene and early Miocene, in response to extensive tectonics.

Menorca is a WNW-ESE elongated island (Figure 3) consisting of two distinct geological domains, separated by a WNW-ESE straight major fault: the northern region (Tramuntana) is made up by Palaeozoic to Cainozoic rocks deformed by Variscan and Alpine phases; the south-western region (Migjorn), consists of Upper Miocene sedimentary covers and subordinate quaternary deposits [49].

The Palaeozoic rocks are mainly represented by unmetamorphosed deposits ranging from the Devonian to the Upper Permian. The Devonian sequence consists of fine-grained clastic terrigenous sediments, mainly sandstone and shales, whose thickness has been estimated at about one thousand meters [49].

The overlaying Carboniferous sequence is represented by terrigenous and calcareous turbidites at the base and turbidites intercalated with fine sandstones at the top [50].

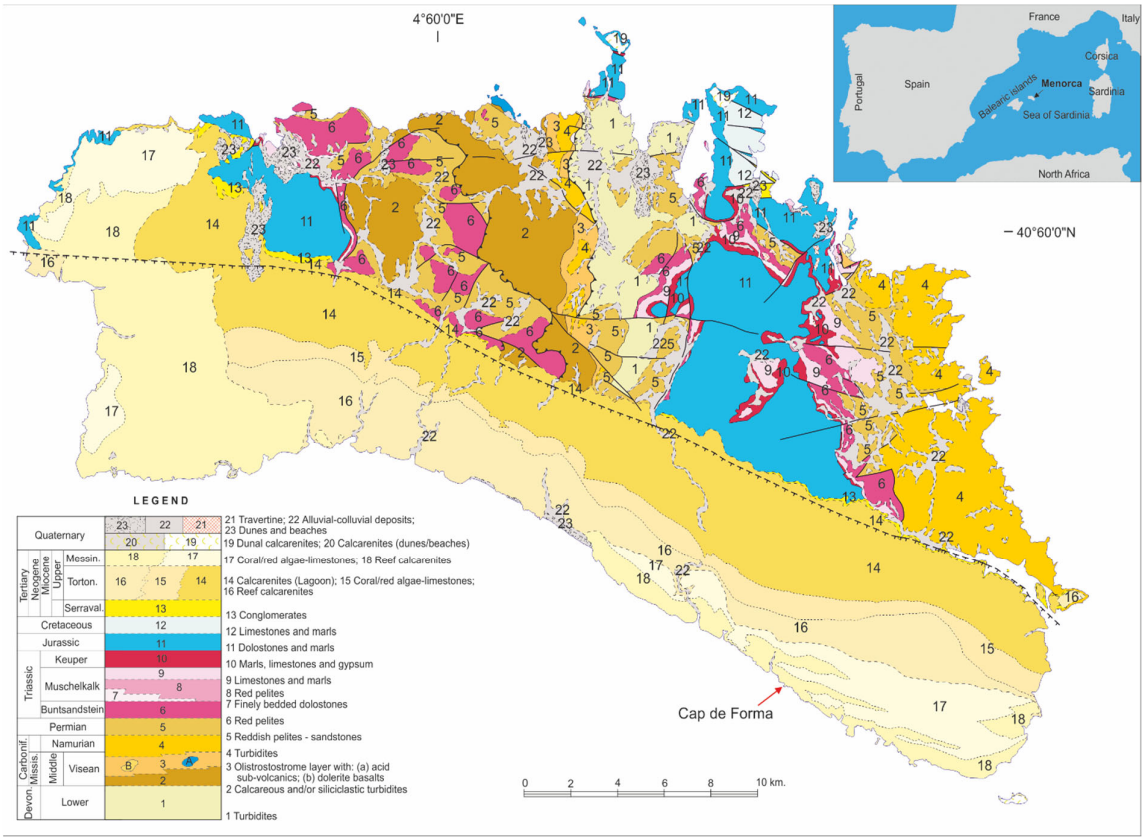

Figure 3. Geological map of Minorca Island at scale 1:100.000. Modified from: [51]. Source ©Instituto Geológico y Minero de España (IGME).

The Permo-Triassic, which forms a 650 m-thick sequence, lies unconformably above the Carboniferous deposits. At the base are layers of clay host sandstone bars and conglomeratic lenses, indicating an alluvial plain environment, of upper Permian age.

An erosive surface marks the transition with the above-lying Triassic sediments showing the typical sequence of Germanic facies: a basal conglomerate is overlain by red shales and sandstone, belonging to the lower Triassic (Buntsandstein), then by middle Triassic carbonates (Muschelkalk) and finally by marls and gypsum of Upper Triassic age (Keuper) [52].

The Jurassic of Menorca is mainly represented by a 300 to 600 m-thick sequence of dolostones and dolomitic limestones, testifying a carbonate sedimentation the persisted till the lower Cretaceous which is characterized by oolithic limestones and marls of 120 m to 400 m in thickness [49]. Upper Cretaceous is totally absent.

The Cenozoic marks the transition to a continental environment starting with thin layers of marsh/lake carbonates of middle Eocene age and going on with Oligocenic alluvial deposits and conoid conglomerates. Lower Miocene rocks are scarce, being limited to few small outcrops of reef limestone alternating with sandstones [53].

On the contrary, the Upper Miocene is widely represented since it covers more than half Menorca's surface from the SE to the NW edges of the island. Two depositional sequences have been recognized [54,55]: the lower one (Tortonian) consists of cross-layered sandstones at the base followed by very bioturbated marly calcarenites, cross-layered grainstones and large scale clinobeds of calcarenites and red algae marls. The upper sequence (Messinian) is a coral reef complex.

The Quaternary deposits of Menorca include marine terraces, alluvial deposits and wind dunes [49].

4. Materials and Methods

4.1. Sampling

A total of 32 samples of mortar and stones (named with code MIN) were taken from main 13 sampling points of the Cap de Forma archaeological complex (Table 1, Figure 4). The samples were taken from an archaeological pit excavated above the Talaotic area and from other ancient structures (e.g., water cistern and the internal environment of the *house-fort*). The materials sampled in the excavated ancient cistern belong to the layers of mortar found on the bottom to seal the cracks in the rock and ensure the watertightness. These mortars were installed in periods following the Talaiotic period. The samples from *house-fort* belong to the materials used for its masonry construction (e.g., inner wall plasters or mortars of ceiling).

Table 1. Macroscopic description of samples taken from the archaeological site of Cap de Forma.

Sampling Points	Sector Strat. Unit	Localis.	Solid/ Powder	Material Description	Layer Nr.	Colour		Xeno-Components
						Surface	Matrix	
MIN1	D4e1 US25	Pit	Solid	Mortar with silicatic aggregate, cocciopesto, with a layer of slightly compacted clay	2	Brown	Layer 1: red; Layer 2: Grey	Combustion traces of clay layer
MIN2	D4e1 US25	Pit	Solid incoherent	Mortar with cocciopesto, silicatic aggregate and lithics	1	Brown	Reddish	Bone/wood fragments
MIN3	D42d US22	Pit	Solid semi-incoherent	Blackish mortar with cocciopesto, silicatic aggregate, limestone fragments	1	Blackish	Whitish	Combustion traces
MIN4	D42d US22	Pit	Solid incoherent	Blackish mortar with cocciopesto, silicatic aggregate, limestone fragments	2	Brown	Layer 1: red; Layer 2: black	Combustion traces
MIN5	D42d US22	Pit	Solid compacted	Limestone with small mortar layer	1	Whitish/ brown	Grey	/
MIN6	D42d US22	Pit	Solid	Fine lime plaster with rare silicatic aggregate, cocciopesto and limestone fragments	1	Whitish/Light brown	Whitish	/
MIN7	D42d US22	Pit	Solid incoherent	Mortar with cocciopesto, silicatic aggregate and lithics	2	Whitish/Light brown	Reddish	Combustion traces
MIN8	D42d US22	Pit	Solid	Fine lime plaster with rare silicatic aggregate, cocciopesto and limestone fragments	2	Light brown	Whitish	/
MIN9	D4e1 US25	Pit	Solid compacted	Fine porous limestone	n.d.	Whitish/Brown/Black	Whitish	/
MIN10	D4e1 US25	Pit	Solid compacted	Fine porous limestone + mortar layer	1 + mortar patina	Strong brown	Grey	Combustion traces
MIN11-1	C7e3-4,d3-4 US153-154	Cistern	Incoherent + fragments	Fine marly limestone	n.d.	Ochre	Beige	/
MIN11-2	C7e3-4,d3-4 US153-154	Cistern	Solid	Cocciopesto mortar with a layer of slightly compacted clay	2	Whitish/Light brown	Whitish	Clay
MIN11-3	C7e3-4,d3-4 US153-154	Cistern	Solid	Cocciopesto fragment	n.d.	Reddish	Reddish	/
MIN12	C7e3-4,d3-4 US153-154	Cistern	Incoherent + small fragments	Cocciopesto mortar with a layer of slightly compacted clay	2	Brown/Blackish	Whitish	Clay
MIN13	A5d5 US134	*House- fort*	Solid	Mortar with silicatic aggregate and binder	1	Whitish/Light brown	Whitish	/

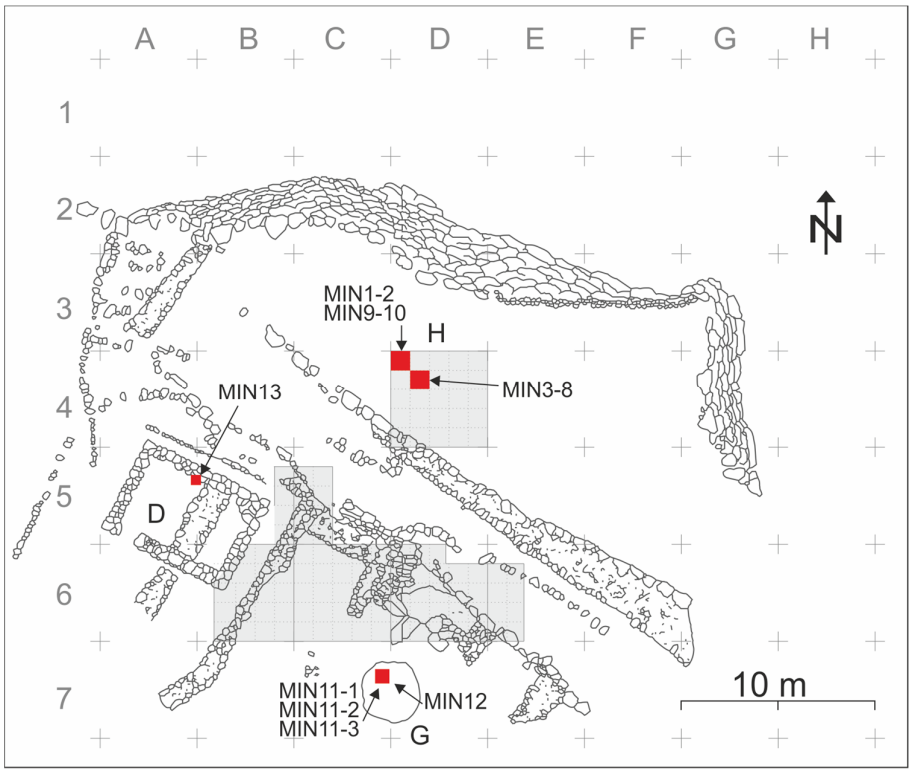

Figure 4. Sketch map of the archaeological site of Cap de Forma, showing the sampling grid and the sampled points (red squares) with the corresponding label (modified after [42]). D = *house-fort*; G = water ancient cistern; H = archaeological dug pit.

In detail, samples MIN1-2 and MIN9-10 located in D4 sector and e1 sub-square (Figure 4) belong to the Stratigraphic Unit (US) 25 (Table 1), which forms part of the filling of the pit (US -27, i.e., archaeological cavity) dug in the upper parts of the structure in a cyclopean technique inside the Talaiotic area. Inside the pit there was, in fact, also other soils with evident traces of combustion (US 21) and the limit between the two US 21 and 25 was not so defined. Samples MIN3-8, on the other hand, located in the nearby D4 sector and d2 sub-square (Figure 4) belong to the wider stratigraphic unit US 22 (which is above the US 25 and US 21) of the pit, which also returned some burnt stones.

Samples MIN11-1, 11-2, 11-3, MIN12 come from the bottom of the ancient water cistern located in the C7 sector between e3-4 and d3-4 sub-squares (Figure 4) and have an abundant fraction of incoherent material represented by clayey earth and only a few fragments of mortars and limestone. The cistern was excavated in the limestone bedrock (US 57), filled with an incoherent deposit of stones and earth (US 56) which, once removed, revealed the presence of a stratigraphic unit consisting of lime incorporating coal and lithic fragments, mixed with loose, soil, of a dark grey colour (US 153), as well as another formation composed of a very compact set of clay, coal and stones (US 154).

Sample MIN13 located in A5 sector and d5 sub-square belongs to US 134 (Figure 4; Table 1) found inside the *house-fort*. This stratigraphic unit consists of a deposit level located within the rectangular environment of the structure characterized by numerous tiles, even whole, by the presence of small quadrangular slabs of sandstone and limestone, with remains of charcoal and fragments of plaster.

4.2. Optical Microscopy and X-ray Diffractometry

Seven thin sections were realized from the most significant samples (MIN1, MIN2, MIN4, MIN8, MIN9, MIN10, MIN13) in order to study the mineralogical and petrographic characteristics by optical microscopy (OM). No petrographic analysis could be carried out

on the samples MIN11 and 12, both represented by an incoherent fraction and by some small compact fragments of limestone, mortar and cocciopesto. Other samples were excluded from thin section preparation to use them in physical-mechanical tests or because they were considered less interesting after the observation in reflected light.

In addition, X-ray diffractometric analyses (XRD) were performed on the samples belonging to MIN2, MIN6, MIN8, MIN10, MIN11, MIN12 and MIN13 sampling points to define the accessory and/or secondary mineralogical phases induced by the samples alteration. Samples selection was driven by the observation under optical microscope and, for incoherent samples, by the impossibility to perform petrographic analyses.

The imaging analysis of the mortars' thin sections at microscopic scale was carried out using the JMicrovision v1.3.3 software to determine the relationships between the binder and the aggregate with grain size on average < 2 mm.

The undisturbed samples of mortar were firstly studied with the optical microscope in reflected light (RL-OM), in order to analyse some compositional aspects of the aggregate and its relationship with the binder, and to observe the characteristics of the surface patinas (such as shape, colour and size of the aggregate), which often provide significant information regarding the degradation processes linked to weathering.

The compositional characteristics and micro-textures were investigated on petrographic thin sections by a JenaLab polarizing optical microscope (PL-OM) (Zeiss, Jena, Germany) and under reflected light (RL-OM) by a Leica S6d (Leica, Wetzlar, Germany), both equipped with a Canon EOS 1200D.

X-ray Diffraction (XRD) was performed on samples previously powdered by an agate mortar, at the Department of Chemical and Geological Sciences (University of Cagliari) by a PANalytical X'Pert Pro diffractometer (Malvern-PANalytical, Almelo, Netherland) equipped with a X'Celerator detector, using the Ni-filtered Cu Kα1 radiation (λ = 1.540598 Å) and theta-theta geometry. Experimental conditions were: acquisition range 5–70°, step-size 0.008°, 0.19 s per step. The operating voltage and current are 40 kV and 40 mA, respectively. The X'Pert HighScore Plus (TM) 2.1.2 software was used for data processing which, through an algorithm, analysed the signals acquired by the detector and recognized the crystalline phases present in the sample by comparison with reference patterns from PDF2 database (release 2010 by ICDD, Newtown Square, PA, USA).

4.3. Physical and Mechanical Tests

Physical and mechanical tests on the mortar/rock samples were performed on a total of 32 centimetre-sized, prismatic specimens, with an average size of 15 mm × 15 mm × 15 mm, cut from the collected samples.

Physical tests were carried out according to [56,57]. The specimens were dried at 105 ± 5 °C and the dry solid mass (m_D) was determined. The solid phases volume (V_S) of powdered rock specimens (on 5–8 g and with particle size less than 0.063 mm) and the real volume (V_R) with:

$$V_R = V_S + V_C$$

where V_C is the volume of pores closed to helium of the specimens was determined by helium Ultrapycnometer 1000 (Quantachrome Instruments). Then, the wet solid mass (m_W) of the samples was determined until constant weight. Through a hydrostatic analytical balance, the bulk volume (V_B) was calculated as:

$$V_B = V_S + V_O + V_C$$

where $V_O = (V_B - V_R)$ is the volume of open pores to helium and V_B is calculated as

$$V_B = \left[\frac{(m_W - m_{HY})}{\rho_{WT}}\right] \cdot 100$$

where m_{HY} is the hydrostatic mass of the wet specimen and ρ_{WT} is the water density at a temperature of 25 °C.

Total porosity (Φ_T), water/helium open porosity ($\Phi_O H_2O$-He), water/helium closed porosity ($\Phi_C H_2O$-He), weight imbibition coefficient (IC_W), saturation index (SI), bulk (ρ_B), real (ρ_R) and solid density (ρ_S) were computed as:

$$\phi_T = \left[\frac{(V_B - V_S)}{V_B}\right] \cdot 100;\ \Phi_{O\ H_2O} = \left\{\frac{\left[\frac{(m_W - m_D)}{\rho_{WTx}}\right]}{V_B}\right\} \cdot 100;\ \ \Phi_{O\ He} = \left[\frac{(V_B - V_R)}{V_B}\right] \cdot 100$$

$$\Phi_{C\ H_2O} = \Phi_T - \Phi_O H_2O;\ \Phi_{C\ He} = \Phi_T - \Phi_O H_e$$

$$IC_w = \left[\frac{(m_w - m_D)}{m_D}\right] \cdot 100;\ SI = \left(\frac{\Phi_O H_2O}{\Phi_O H_e}\right) = \left\{\frac{\left[\frac{(m_W - m_D)}{\rho_{WTx}}\right]}{V_O}\right\} \cdot 100$$

$$\rho_S = \frac{m_D}{V_S};\ \rho_R = \frac{m_D}{V_R};\ \rho_B = \frac{m_D}{V_B}$$

The punching strength index (PLT index) was determined with a Point Load Tester (mod. D550 Controls Instrument), according to ISRM Recommendations [58,59]. The puncturing resistance index (Is) was calculated as:

$$Is = \frac{P}{De^2}$$

where P is breaking load and De the "equivalent diameter of the cylindrical specimen" (ISRM, 1972, 1985) with:

$$De = \frac{4A}{\pi};\ A = W \cdot D$$

where W and 2L are the width perpendicular to the load direction and length of specimen, respectively, and D is the distance between the two conical punches. The index value is referred to a standard cylindrical specimen with diameter D = 50 mm for which it has been corrected with a shape coefficient (F) and calculated as:

$$Is_{(50)} = Is \cdot F = Is \cdot \left(\frac{De}{50}\right)^{0,45}$$

4.4. Binder/Aggregate Ratio by Imaging Analysis

The ratio between binder and aggregate (B/A ratio) of the mortars was determined by the software JMicrovision v1.3.3 [60], useful for carrying out imaging analysis obtained from the polarizing microscope (IA-OM) and designed to describe and measure, quantify and classify all components.

The binder and aggregate amounts were determined by the "Point Counting" tool that assigns a class to each measured point. Three classes were distinguished by three different colours: binder in red; aggregates in green; the pores in yellow. By setting the total count of points on the image to 750 units, the different percentages of each class set on JMicrovision were determined.

5. Results

5.1. Mineralogical and Petrographic Characteristics of Mortars

Data of the compositional characteristics of mortars and stones sampled from the archaeological complex of Cap de Forma are shown in Table 2, which summarizes the results of macroscopic and mesoscopic analyses under reflected light microscope (RL-OM), the microscopic analyses in polarized light (PL-OM) and the diffractometric ones on powdered samples (XRD; Figure 5).

Table 2. Results of microscopic (PL-OM) and X-ray diffractometric (XRD) analysis of the samples taken from the pit and a stratigraphic layer up to the cyclopic construction area, from the cistern and from the *house-fort* of the archaeological site of Cap de Forma.

Sample	Site	Group	Material Type	Imaging Analysis		Microscopic Analysis (PL-OM)	Minerals by XRD Analysis	
				Aggregate %	Binder %	Components	Aggregate	Binder
MIN2	Pit	P1	Mortar	28.1	70.9	cocciopesto, quartz, limestone lithics, rare feldspar	Qtz, Cal, Dol, Arg	Cal
MIN7	Pit	P1	Mortar	n.d.	n.d.	cocciopesto, quartz, lithics	n.d.	n.d.
MIN3	Pit	P2a	Mortar	n.d.	n.d.	cocciopesto, quartz, limestone lithics	n.d.	n.d.
MIN4	Pit	P2a	Mortar	35.8	58.3	quartz, cocciopesto, calcareous lithics	n.d.	n.d.
MIN1	Pit	P2b	Mortar	16.3	76.3	quartz, rare feldspar and biotite, cocciopesto, limestone lithics	n.d.	n.d.
MIN6	Pit	P3	Mortar	n.d.	n.d.	quartz, cocciopesto	Qtz, Cal, Dol	Cal, Per
MIN8	Pit	P3	Mortar	4.8	92.5	quartz, cocciopesto, limestone fragments	Qtz, Cal, Dol	Cal, Per, (Mgs)
MIN9	Pit	P4a	Limestone/Mortar	n.d.	n.d.	microcrystalline calcite (in limestone), quartz (in mortar layer)	n.d.	n.d.
MIN10	Pit	P4a	Limestone/Mortar	4.9	89.6	microcrystalline calcite (in limestone), quartz and cocciopesto (in mortar layer)	Cal, Dol, Mag	Cal
MIN5	Pit	P4b	Mortar/Limestone	10.1	84.8	microcrystalline calcite (in limestone), cocciopesto (in mortar layer)	n.d.	n.d.
MIN12	Cistern	C1	Cocciopesto	n.d.	n.d.	n.d.	Qtz, Cal, Dol, Arg, Fsp, Bt	Cal
MIN11-2	Cistern	C1	Mortar	n.d.	n.d.	n.d.	n.d.	n.d.
MIN11-3	Cistern	C2	Cocciopesto	n.d.	n.d.	n.d.	n.d.	n.d.
MIN11-1	Cistern	C3	Limestone/Mortar	n.d.	n.d.	n.d.	Qtz, Cal, Dol, Fsp, Bt	Cal
MIN13	*House-fort*	H	Mortar	28.2	66.1	brown lithic not identified, fibrous mineral (gypsum), quartz, mafic minerals (?)	Qtz, Dol	Bas, Anh, Mgs

Abbreviation legend: Qtz = quartz, Cal = calcite, Dol = dolomite, Arg = aragonite, Fsp = feldspar, Bt = biotite, Bas = bassanite, Anh = anhydrite, Mgs = magnesite, Per = periclase, n.d. = not determined.

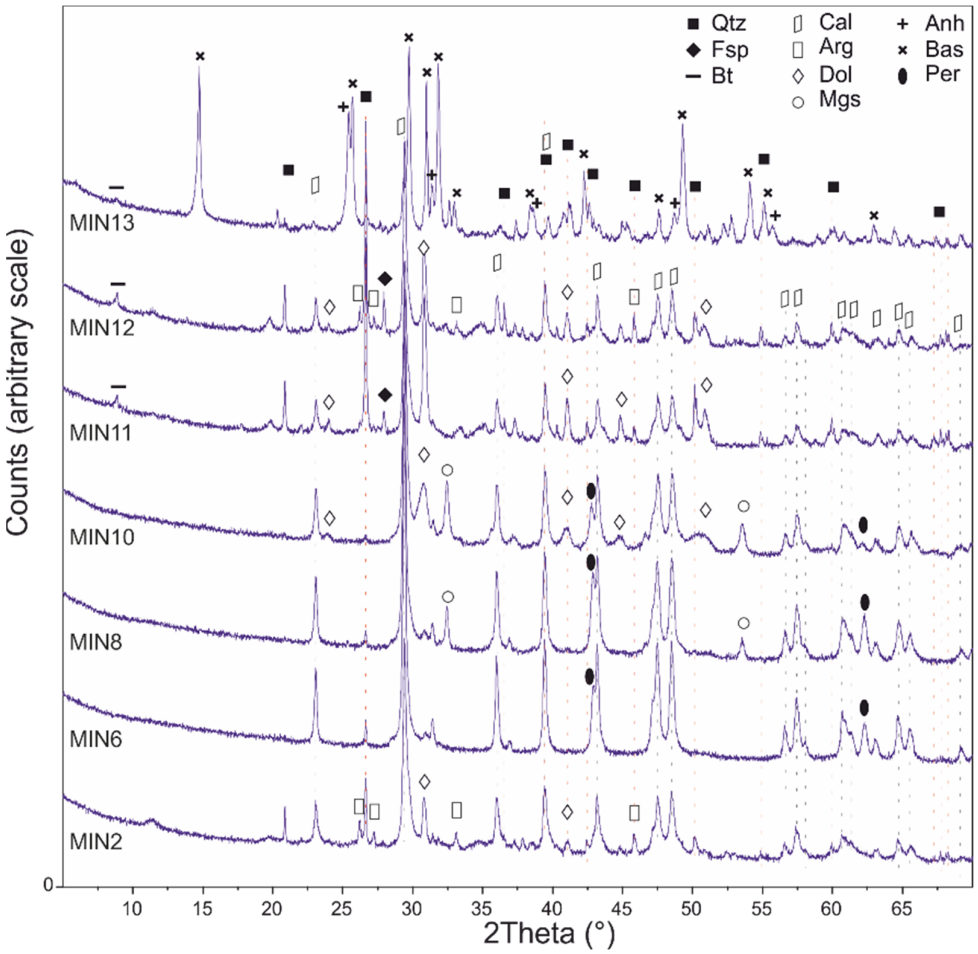

Figure 5. Synoptic XRD diagram showing the patterns of the analysed samples. Excluding the MIN13 sample which has a chalky binder (with bassanite and anhydrite), the presence of a calcitic binder is noted in all the samples studied. As for the aggregate, the XRD analysis shows the presence of dolomite and quartz as common minerals between the various samples. Subject to these, among the various samples there is the presence of aragonite (polymorph of calcite), periclase and magnesite (related to the presence of dolomite), biotite and albite. Mineral abbreviations: Qtz = quartz, Cal = calcite, Dol = dolomite, Arg = aragonite, Fsp = feldspar, Bt = biotite, Bas = bassanite, Anh = anhydrite, Mgs = magnesite, Per = periclase, n.d. = not determined.

The binder/aggregate ratios measured by JMicrovision are commonly very high leading to the preliminary hypothesis that almost all samples were plaster mortars or, in any case, coating mortars. However, it should be emphasized that these ratios are obtained from images at the microscopic scale and that therefore the IA-OM analysis does not include the coarse fraction of the aggregate (>1 cm) and the very fine fraction (<200 μm), which is certainly well represented, especially in some of these mortars. The values of the binder/aggregate ratio, which on a microscale are around 2: 1, on a macroscopic scale are undoubtedly lower, probably around 1: 1, or even in some cases inverted, i.e., equal to 1: 2.

Samples have been gathered in groups according to the sampling point (P = archaeological dug pit; C = ancient cistern; H = *house-fort*) and in subgroups on the basis of the compositional aspects observed at macroscopic (millimetre), mesoscopic (sub-millimetre) and microscopic scales, as follows:

Pit sector

Group P1—Mortars with silicate (Qtz, Fsp) aggregate, cocciopesto and lithics, with 28 vol% (Table 2) of aggregate (samples MIN2-1, 2-2, e MIN7-1, 7-2, 7-3, 7-4, 7-5);

Group P2—Blackish mortars with silicate aggregate, cocciopesto, limestone fragments and combustion traces, divided in P2a subgroup mortars with 36 vol% of aggregate (MIN3-1 e MIN4-1, 4-2, 4-3) and P2b subgroup mortars with a layer of slightly compacted clay and combustion traces and with 16 vol% of aggregate (MIN1-1, 1-2, 1-3, 1-4);

Group P3—Fine lime plasters with rare silicates (main Qtz) and cocciopesto aggregate and limestone fragments, with 5 vol% of aggregate (MIN6-1, 6-2 e MIN8-1, 8-2, 8-3);

Group P4—Limestone divided in P4a subgroup of MIN5-1 and MIN5-2 samples and P4b subgroup of fine porous limestones with calcite and dolomite (MIN9-1 and MIN10-1).

Cistern sector

Group C1—Incoherent materials represented by cocciopesto mortar fragments with slightly compacted clay (MIN11-2, MIN11-5, e MIN12-1), with very similar composition to the P2b mortar:

Group C2—Cocciopesto fragment (MIN11-3 e 11-4);

Group C3—Fine marly limestone (MIN11-1).

House-fort sector

Group H—Mortars with lime/gypsum binder and silicate aggregate, with 28 vol% of aggregate (MIN13-1, 13-2).

5.1.1. Samples from the Pit

Group P1—Cocciopesto Mortar (Samples MIN2, MIN7)

Under reflected light optical microscopy (RL-OM), MIN2 and MIN7 are quite similar, but with a higher amount of aggregate, mainly consisting of reddish grains ranging from sub- to millimetre size (Figure 6a,b), and greyish lithics up to about 1 cm, in the former. MIN7 sample is characterized by the presence of very fine reddish aggregates, generally ranging between 100 μm and 200 μm but occasionally reaching 2 mm. Both samples are characterized by a whitish binder with millimetre-sized lime lumps. Locally, a very thin, very friable blackish layer is observed.

The imaging analysis obtained with a polarizing microscope (IA-OM) shows a Binder/Aggregate (B/A) ratio of 28.1/70.9% in the MIN2 sample, with a low porosity at the microscopic scale of 0.9% (Table 2). Polarizing microscope observation (PL-OM, Figure 6c–f) confirms that most of the aggregate is represented by cocciopesto fragments. They show a quartz-based skeleton and a colour varying from reddish to dark brown to grey blackish in colour, presumably due to the different cooking conditions (oxidizing/reducing). The fragment size ranges from 2–3 mm in the larger ones to 100–200 μm in the smaller ones.

In addition to the cocciopesto the aggregates are represented by tiny crystals of quartz and rare feldspar with an average size of about 100–200 μm, rare millimetre-sized limestone fragments and a single chip an original bone or wood (Figure 6c,d). The presence of dark-coloured organic material (about 100 μm) is probably referable to carbon residues deriving from the limestone calcination during the production of lime.

The binder is substantially lime based; it has a microcrystalline texture with a calcite composition. The presence of lime lumps of about 10–20 μm, but reaching about 1 mm, can be noted. Close to the contact with the fragments of cocciopesto, very thin edges (<15 μm) of a pale red colour are observed, probably indicating a partial reaction with the binder.

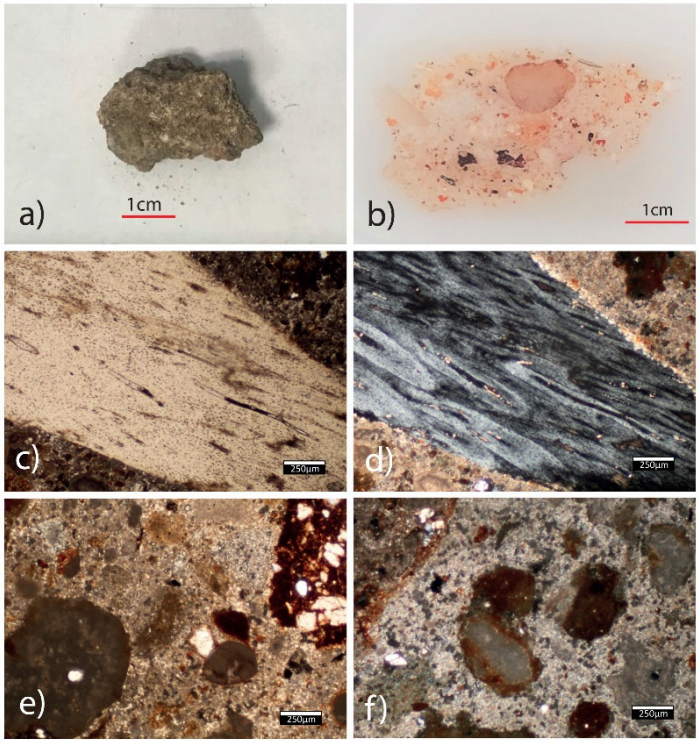

Figure 6. Sample MIN2 (Group P1) microphotographs under polarised light microscopy (PL-OM). Mortar with cocciopesto, quartz/feldspar aggregate and lithics. (**a**) analysed fragment; (**b**) thin section of sample where there is a limestone fragment and a coarse, not identified aggregate; (**c**) parallel polars and (**d**) crossed polars: organic fragment (probable bone or plant tissue) immersed in the mortar; (**e**) parallel polars: lime lump (down left) and cocciopesto fragment with quartz microcrystals inside (**f**) crossed polars: aggregates immersed in mortar binder.

Group P2a—Blackish Cocciopesto Mortar (MIN3, MIN4)

MIN3 and MIN4 samples (Figure 7a,b) have a dark greyish/blackish matrix with evident lime lumps. Aggregate consists of quartz and dark cocciopesto in MIN4 and of reddish cocciopesto in MIN3.

MIN4 is subdivided into two layers of different colours; the external layer (2 cm-thick) is dark brown to black probably due to a combustion process occurring near the mortar, whereas the inner one (few mm) is lighter tending to reddish. PL-OM analysis (Figure 7c–h) revealed that not only the burning event produced the darker colour of the external layer; indeed, it shows a cocciopesto-rich aggregate of average size of about 1 mm and subordinate smaller quartz crystals (150–200 µm). The presence of various millimetric calcareous lithics with fossiliferous content is also observed; they probably belong to the badly burnt raw limestone and/or to limestone fragments used as aggregates. Evidence of incomplete slaking of CaO is also observed, as testified by microscopic lumps of lime (now carbonated) within some limestone fragment. The mortar layer with lighter colour is characterized by a lower presence of aggregate with smaller size (in the range 50–200 µm), mainly represented by small quartz crystals, while the remainder is made up of fragments of cocciopesto. In this case also, the calcite binder has a microcrystalline texture with lime lumps and fossiliferous scraps sometimes showing reaction/re-sorption edges with the surrounding binder matrix. In mortar there are shrinkage micro-cracks (30–40 µm, Figure 7c–h), probably induced by the combustion process, which involved the mortar after it was applied.

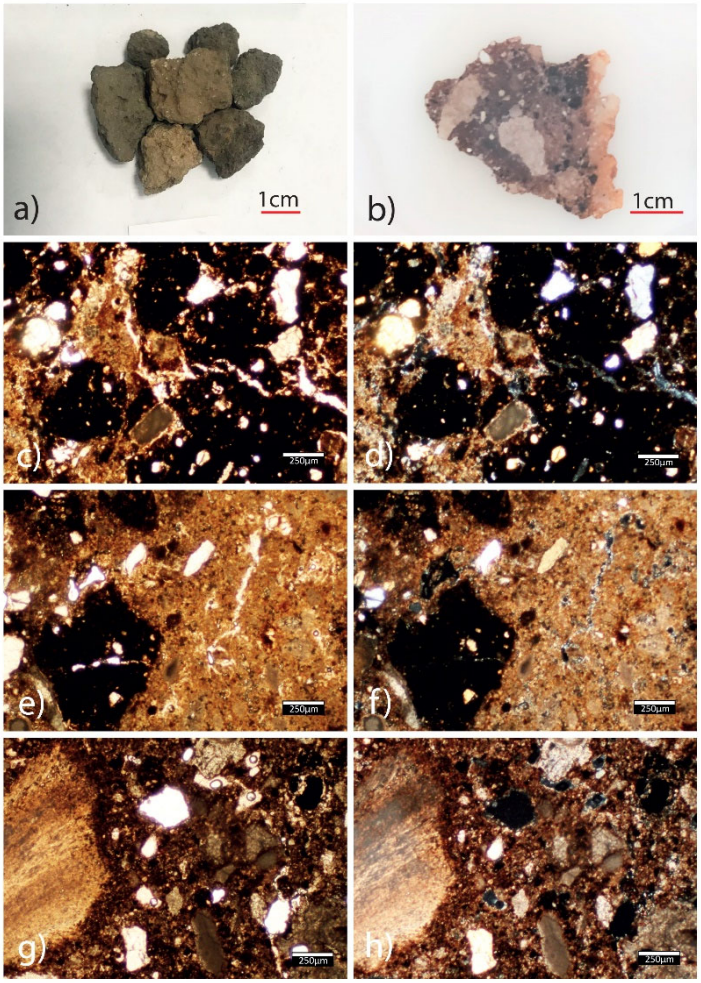

Figure 7. Sample MIN4 (Group P2a) microphotographs under polarised light microscopy (PL-OM). Blackish mortar with dark and reddish cocciopesto, silicatic aggregate, limestone fragments and combustion traces. (**a**) analysed fragments; (**b**) thin section where there is a transition in the mortar between a dark area (affected by combustion processes) and a light reddish area referable to the undisturbed part of the sample; (**c**) parallel polars and (**d**) crossed polars: fragments of dark and reddish cocciopesto with quartz and feldspar microcrystals inside; (**e**) parallel polars and (**f**) crossed polars: transition in the mortar between dark area and light reddish area; (**g**) parallel polars and (**h**) crossed polars: crystal-clasts of quartz, calcareous lithics and other aggregate lithic fragment in the dark zone of mortar. In microphotos c-h there are shrinkage micro-cracks probably induced by a combustion.

The MIN3 sample has an aggregate with a grain size distribution in the range of fine sands where the largest fragments, few and scattered, reach a maximum size of 200 µm, and there is reddish cocciopesto. Furthermore, the calcitic binder appears not very compact and friable, where some lumps of lime with size lower than 500 µm are immersed.

IA-OM analysis of MIN4 shows a B/A ratio (%) of the aggregate of 58.3/35.8% and a microscopic porosity of 5.9% (Table 2).

Groups P2b—Cocciopesto Mortars with Compacted Clay (MIN1)

A macroscopic observation of the MIN1 sample (Figure 8a) shows the presence of two layers. The first (probably innermost), with a thickness between 7 and 10 mm, has an aggregate with a reddish colour due to the presence of abundant cocciopesto fragments.

The second layer shows a darker colour, locally grey or black on the surface due to the presence of microscopic fragments of coal and/or by the deposition of unburnt carbon particles. Lime lumps are observed.

The IA-OM analysis of the MIN1 sample shows a B/A (%) ratio of 76.3/16.3%, with a microscopic porosity of 7.5% (Table 2).

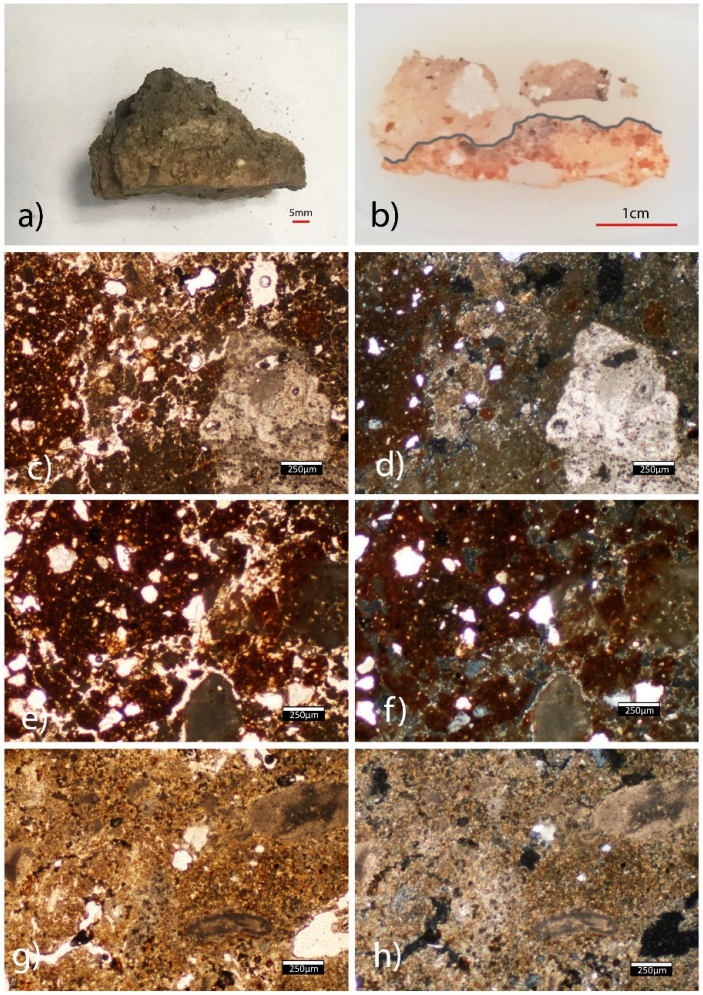

Figure 8. Sample MIN1 (Group P2b) microphotographs under polarised light microscopy (PL-OM). Mortar with cocciopesto and silicatic aggregate with a layer of slightly compacted clay and combustion traces. (**a**) analysed fragment; (**b**) thin section with stratification in two layers: cocciopesto mortar (lower layer) and mortar with a few pluri-millimetric fragments of limestone (upper layer); (**c**) parallel polars and (**d**) crossed polars: cocciopesto, quartz, feldspars, and a limestone fragments in mortar aggregate; (**e**) parallel polars and (**f**) crossed polars: cocciopesto, quartz and a lime-lump; (**g**) parallel polars and (**h**) crossed polars: microcrystalline calcitic binder.

The PL-OM observation (Figure 8c–h) shows an inhomogeneous distribution of the aggregate throughout the section. The first layer has a large amount of cocciopesto fragments, ranging in size from 900 to 1500 µm, hosting quartz crystals, rare feldspar and occasional biotite crystals. In addition to the cocciopesto, there are some multi-millimetric fragments of dolomitic limestone containing fossils and crystals of quartz and feldspar with dimensions ranging from 300 to 1000 µm. In the second layer (outermost, probably representing the finishing mortar), there is the same type of aggregate but in smaller quantities and sizes, especially as regards the fragments of cocciopesto, which have dimensions between 400 and 500 µm.

The lime-based binder has a microcrystalline texture and a homogeneous structure. The presence of large lumps indicates a not unorthodox way of extinguishing lime.

Group P3—Fine Lime Plaster with Rare Cocciopesto (MIN6, MIN8)

The MIN6 mortar sample is macroscopically porous and incoherent, with a high number of lime lumps very clear and crumbly (Figure 9a).

RL-PL-OM analysis highlights a calcitic binder and an aggregate consisting of small crystals of quartz (200 μm), and of cocciopesto with a generally very fine grain (200 μm), with few exceptions reaching up to 1 mm. The very fine grain of the aggregate suggests that this mortar probably was part of a plaster.

The XRD analysis shows the prevalent presence of calcite (essentially referable to the binder), quartz and traces of periclase (MgO) and dolomite whose significance is discussed in the Discussion section.

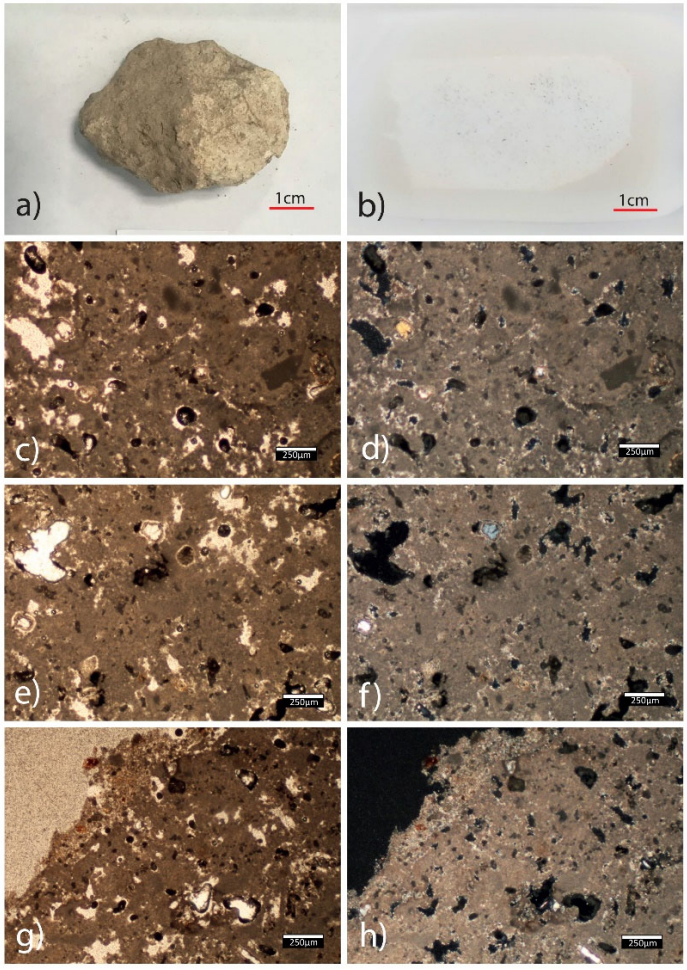

Figure 9. Sample MIN8 (Group P3) microphotographs under polarised light microscopy (PL-OM). Limestone fragments with residue of fine lime plaster. (**a**) analysed fragment; (**b**) homogeneous thin section; (**c**,**e**) parallel polars and (**d**,**f**) crossed polars: microcrystalline calcitic matrix; (**g**) parallel polars and (**h**) crossed polars: residue of fine lime plaster with quartz and cocciopesto aggregate (top left of photo).

MIN8 sample (Figure 9a,b) consists of a fragment of limestone and a thin layer of mortar adhering to the limestone. Macroscopic analysis sample shows a compact and homogeneous whitish fragment. From a first preliminary investigation on a meso-microscopic scale (RL-OM), no type of aggregate is evident. This, together with the absence of

fossils, leads us to think that it is a fragment of limestone belonging to the substrate on which the mortar was applied or a fragment of limestone not completely burnt, resulting from the production of lime.

The PL-OM analysis of the MIN8 sample (Figure 9c–f) shows the high homogeneity of the limestone fragment with a carbonate composition, within which an isotropic distribution of porosity with a pore size of about 60–120 μm is observed. In addition to these, some small and rare scattered quartz crystals (20–30 μm) can be recognized, indicating that it may be a weakly arenaceous limestone (i.e., calcarenite) rather than pure limestone [54]. The XRD analysis shows the presence of some peaks in the diffractogram that are not well identified, probably attributable to magnesite (Figure 5). The thin layer of mortar (about 400–500 μm, Figure 8g,h) adhering to the limestone fragment is characterized by the presence of few fragments of cocciopesto with dimensions between 50 and 150 μm.

Group P4—Limestone Samples from the Mortars (MIN5, MIN9, MIN10)

The MIN5 belonging to the subgroup P4a is a rock sample showing a whitish colour and high compactness. On the surface there is a thin layer of mortar (belonging to the aforementioned mortars) characterized by an aggregate mainly of cocciopesto (100–200 μm) and by the presence of a possible lump of lime (very white and crumbly).

The MIN9 sample of subgroup P4b shows macroscopically a marked yellowish colour (Figure 10a) and is coated by a thin superficial blackish layer (Figure 10b); it represents a fragment of limestone resulting from the production of lime, in which there is a residue of an original mortar characterised by blackish, yellowish and reddish aggregates (this latter referable to cocciopesto) with a homogeneous size, with some rare quartz microcrystals (less than 50 μm). There are lumps of lime highlighting an unorthodox processing and firing of the limestone.

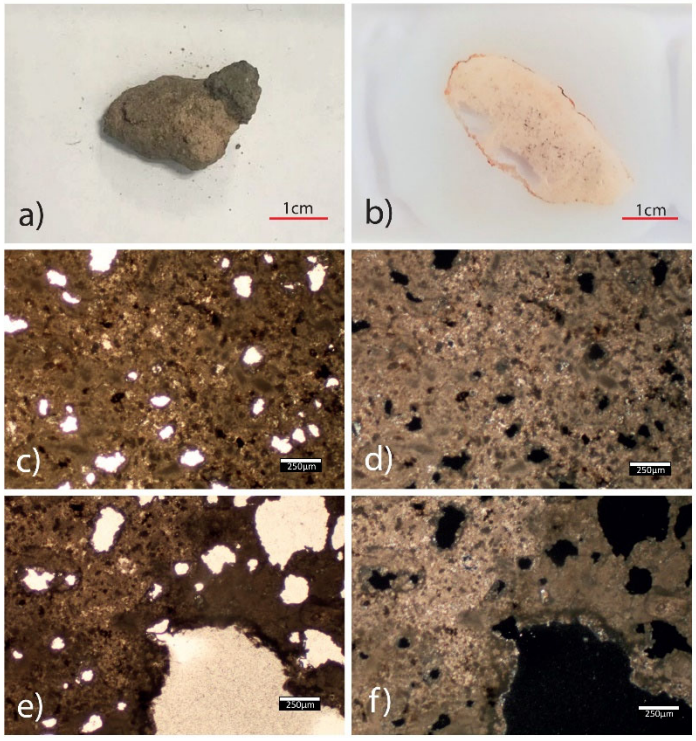

Figure 10. Sample MIN9 (Group P4b) microphotographs under polarised light microscopy (PL-OM). Limestone samples with lime plaster thin layer. (**a**) analysed fragment; (**b**) homogeneous thin section with a thin layer around the fragment with different composition; (**c**) parallel polars and (**d**) crossed polars: microcrystalline calcitic matrix; (**e**) parallel polars and (**f**) crossed polars: variable porosity on lime plaster matrix with size frequently from 70 up to 1200 μm.

The MIN10 sample (Figure 11a) of subgroup P4b macroscopically appears very homogeneous with a greyish colour; it is very hard but with an apparently porous structure. There are two blackish residues of mortar with a thickness of 2–3 mm (Figure 11b). The mortar shows the only visible aggregates, consisting of very fine quartz and earthenware. On the surface there is also the presence of a very thin and crumbly blackish layer, presumably due to combustion residues.

Microscopically (from PL-OM, Figure 11c–f) the mortar appears rich in cocciopesto (200 μm) with subordinate crystal-clasts of quartz, within a calcitic binder. Microcrystals of calcite at the edges of the pores, probably formed by secondary precipitation, were also observed.

Through the XRD analysis, the presence of calcite, dolomite and magnesite is revealed (Figure 5). The presence of magnesite ($MgCO_3$) appears odd in itself but could be associated with the high presence of the same dolomite.

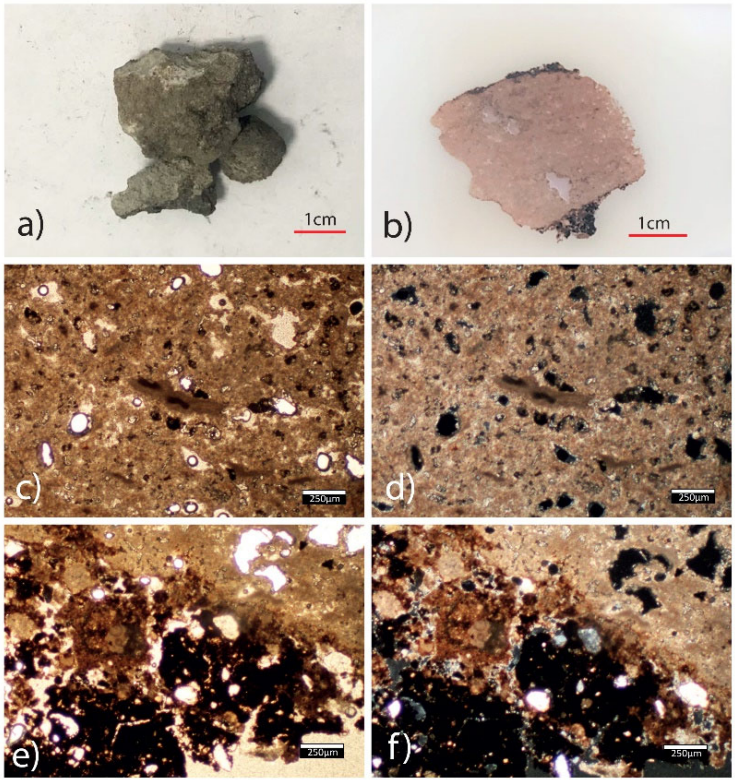

Figure 11. Sample MIN10 (Groups P4b) microphotographs under polarised light microscope (PL-OM). Limestone samples with dark residue of cocciopesto mortar. (**a**) analysed fragment; (**b**) thin section; (**c**) parallel polars and (**d**) crossed polars: microcrystalline calcitic matrix; (**e**) parallel polars and (**f**) crossed polars: contact between the limestone fragment and dark cocciopesto mortar.

5.1.2. Samples from the Ancient Water Cistern

MIN11 and MIN12 samples are represented by an incoherent fraction with small compact fragments of mortar, cocciopesto and limestone.

The macroscopic analysis of mortar fragments highlights the presence of a reddish and greyish aggregate immersed in a homogeneous binder matrix.

By RL-OM mesoscopic observations the mortar fragments show a B/A (%) ratio of about 70/20%, with a microscopic porosity of 8–10%. Due to the small size of the mortar fragments, this analysis is obviously approximate especially since the fraction of the aggregate that cannot be resolved at the mesoscopic scale is not counted. The reddish aggregate is represented by the cocciopesto fragments ranging in size from 0.7 to 3 mm. Quartz

crystals, rare feldspar and occasional biotite crystals are also observed, with dimensions ranging from 0.4 to 2 mm. In addition, there are some millimetric lithoclasts of limestone. In some mortar samples an aggregate with smaller size and lower amount is observed, probably representing a finishing mortar (or plaster), especially as regards the cocciopesto fragments, ranging from 0.5 to 1.5 mm.

The binder is lime based with whitish colour. Occasional mortar fragments with greyish and blackish coloured binder are also present in both samples, mainly due to the presence of microscopic unburnt carbon particles and occasional coal fragments. In addition, lime lumps are observed in the binder.

XRD analyses of MIN11 sample confirm what was observed in RL-OM analysis, i.e., the presence of calcite (ascribable both to the main phase of lime binder and the limestone fragments in the aggregate), dolomite (that refers to limestone), quartz and traces of albite (i.e., plagioclase) and biotite (Figure 5). The MIN12 sample shows the presence of quartz, calcite, dolomite and aragonite, with traces of biotite and albite. In addition to these minerals, further peaks not assigned to any mineralogical phase were detected.

5.1.3. Samples from the House-Fort

Group H—Mortar with Lime/Gypsum Binder (MIN13)

The specimen MIN13 is about 5 cm in size and has a flattened shape (Figure 12a). Macroscopically, an aggregate with colours ranging from light grey to reddish can be seen, attributable respectively to crystal clasts of sialic minerals and cocciopesto fragments generally ranging in size between 400 μm and 1 mm immersed in a whitish binder matrix.

The imaging analysis (IA-OM) shows a B/A ratio of 66.1/28.2%, with a microscopic porosity of 5.7% (Table 2).

Through the RL-OM observation, different types of aggregate are recognized such as cocciopesto, quartz and feldspar. The average size of aggregate is 50–100 μm with a maximum size of about 500 μm. The binder is carbonatic with the presence of lime lumps (very clear and crumbly).

PL-OM analysis of the aggregate (Figure 12c–h) highlights the presence of brown and sub-rounded lithic fragments with size between 100 and 900 μm, while quartz usually do not exceed 100 μm. The presence of mafic (?) minerals with a maximum size of 500 μm is also a possibility. In addition to these phases, another widespread mineral was detected; it forms clusters of 700 μm–1.5 mm consisting of a set of needle-like phases (Figure 12g,h), which are not well resolvable under the microscope.

The binder shows a microcrystalline structure with several lumps of lime with dimensions of about 200 μm. The mineralogical phases found by XRD analysis (Figure 5) are: bassanite (gypsum hemihydrate, $CaSO_4 \bullet 0.5H_2O$), anhydrite ($CaSO_4$), dolomite with subordinated quartz and magnesite. Bassanite and anhydrite probably represent the fibrous mineralogical species with high interference colours observed under the polarizing microscope (PL-OM).

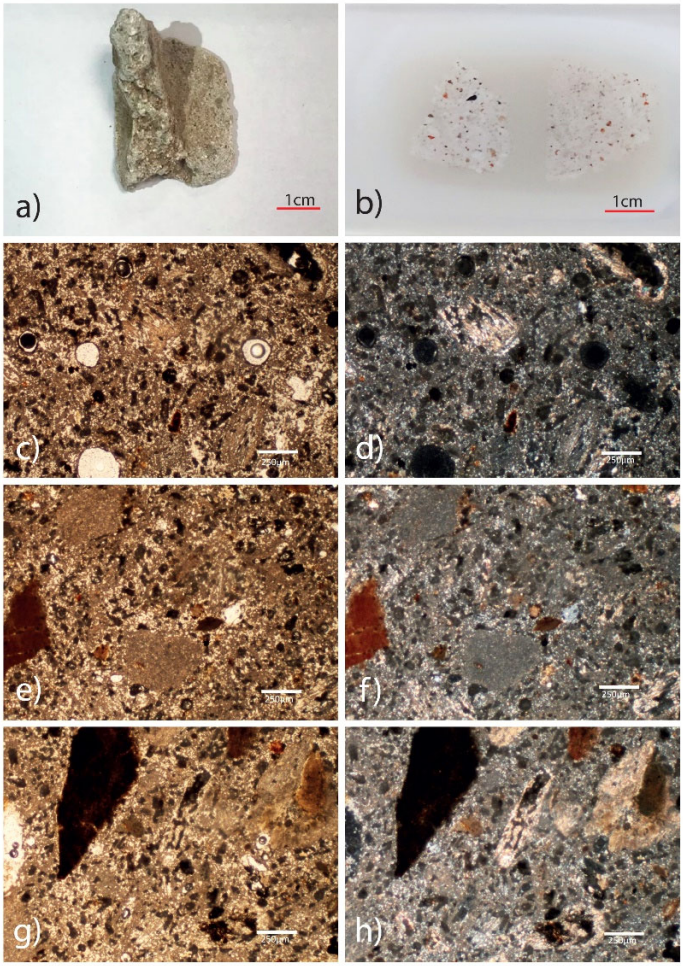

Figure 12. Sample MIN13 (Group H) microphotographs under polarised light microscopy (PL-OM). Mortar with silicatic aggregate and lime/gypsum binder. (**a**) analysed fragment; (**b**) thin section where is visible a fine aggregate (mainly silicatic); (**c**) parallel nicol and (**d**) crossed polars: lime/gypsum binder with silicatic aggregate immersed in the matrix and there is a needle-like mineral species (gypsum); (**e**) parallel polars and (**f**) crossed polars: silicatic aggregate and cocciopesto fragment; (**g**) parallel polars and (**h**) crossed polars: orange cocciopesto and needle-like gypsum crystal (best visible in (**h**).

5.2. Physical-Mechanical Features of Mortars

For a complete characterization of the analysed materials (i.e., bedding mortars, cladding, rocks, various fragments), the following fundamental physical properties were determined: real density, bulk density, open porosity to helium, open and closed porosity to water, imbibition coefficient (expressed in weight), saturation index, punching resistance index and indirectly also the compressive and tensile strengths (Tables 3 and 4).

The different compositional characteristics of the groups of geomaterials described in the previous paragraph consequently reflect different physical and mechanical properties. Figure 13 shows the graphs that plot the data (Table 3) of the main physical properties determined. In Figure 13a, which shows the open porosity to helium against the bulk density, it is observed that the cocciopesto mortars have high variability (32–60%, Table 3) of the open porosity (i.e., interconnected), induced, on the one hand, by the compositional heterogeneity and, on the other hand, by the deterioration of the mortars. The open porosity to water, albeit with slightly lower values, shows a trend similar to that of open porosity to helium. The high porosity of the samples results in extremely low values of the bulk density, between about 1.85 and 1.05 g/cm^3 (Table 3).

Table 3. Physical properties of samples taken from Area B and *house-fort* of Cap de Forma archaeological site.

Sample	Groups	Aggregate	ρ_R	ρ_B	Φ_O He	Φ_O H_2O	Φ_C H_2O	IC_W	SI
		(%)	(g/cm³)	(g/cm³)	(%)	(%)	(%)	(%)	(%)
MIN 2-1	Group P1	28	2.57	1.13	56.0	50.9	5.0	45.0	91.0
MIN 2-2		30	2.61	1.04	60.0	59.3	0.7	56.7	98.8
MIN 7-1		27	2.69	1.13	57.9	52.8	5.0	46.5	91.3
MIN 7-2		32	2.59	1.23	52.5	40.6	11.9	33.0	77.2
MIN 7-3		29	2.55	1.16	54.6	47.6	7.0	41.1	87.1
MIN 7-4		31	2.66	1.12	57.9	50.0	8.0	44.6	86.3
MIN 7-5		28	2.64	1.17	55.7	52.5	3.2	44.9	94.3
MIN 3-1	Group P2a	37	2.66	1.39	47.5	46.8	0.7	33.5	98.5
MIN 4-1		36	2.68	1.38	48.5	45.6	3.0	32.9	93.9
MIN 4-2		34	2.68	1.41	47.3	46.7	0.6	33.0	98.7
MIN 4-3		38	2.67	1.49	44.3	35.3	9.0	23.7	79.6
MIN 1-1	Group P2b	16	2.51	1.45	42.1	37.4	4.7	25.7	88.9
MIN 1-2		17	2.63	1.37	48.0	47.0	0.9	34.4	98.0
MIN 1-3		20	2.62	1.45	44.7	43.8	0.9	30.2	97.9
MIN 1-4		16	2.64	1.44	45.4	42.4	3.0	29.4	93.4
MIN 6-1	Group P3	5	2.64	1.10	58.3	55.5	2.8	50.3	95.2
MIN 6-2		7	2.62	1.06	59.6	56.7	2.8	53.5	95.2
MIN 8-1		5	2.63	1.45	44.9	40.3	4.6	27.8	89.7
MIN 8-2		7	2.66	1.40	47.3	35.3	11.9	25.1	74.8
MIN 8-3		6	2.67	1.47	44.8	38.6	6.3	26.1	86.0
MIN 9-1	Group P4a	n.d.	2.69	1.26	53.2	44.8	8.3	35.5	84.3
MIN 10-1			2.70	1.53	43.2	38.0	5.2	24.8	87.9
MIN 5-1	Group P4b	n.d.	2.71	2.09	23.0	18.3	4.7	8.8	79.6
MIN 5-2			2.70	2.11	21.8	19.0	2.9	9.0	86.9
MIN 11-2	Group C1	33	2.61	1.16	55.6	52.5	3.0	45.2	94.6
MIN 11-5		31	2.68	1.31	51.0	42.3	8.7	32.1	82.9
MIN 12-1		30	2.69	1.85	31.3	30.7	0.6	16.6	98.1
MIN 11-3	Group C2	n.d.	2.41	1.19	50.6	25.2	25.5	21.1	49.7
MIN 11-4			2.47	1.29	47.6	22.1	25.5	17.0	46.4
MIN 11-1	Group C3	n.d.	2.69	1.23	54.2	36.4	17.8	29.5	67.1
MIN 13-1	Group H	28	2.75	1.42	48.4	39.2	9.2	27.6	81.0
MIN 13-2		29	2.76	1.47	46.8	23.6	23.2	16.0	50.4

Abbreviation legend: B = binder vol.%; ϱ_R = real density; ϱ_B = bulk density; Φ_O He = helium open porosity; Φ_O H_2O = water open porosity; Φ_C H_2O = water closed porosity; IC_W = water imbibition coefficient; SI = water saturation index; n.d. = not determined.

Table 4. Data of mechanical Point Load Test of samples belonging to Area B and *house-fort* from Cap de Forma archaeological site.

Sample	Groups	P	W	H	De^2	De	Is	F	$Is_{(50)}$	R_C		R_T	
		(N)	(mm)	(mm)	(mm²)	(mm)	(N/mm²)	/	(MPa)	(MPa)	(kg/cm²)	(MPa)	(kg/cm²)
MIN 2-1	Group P1	0.15	1.40	1.25	2.23	1.49	0.07	0.21	0.01	0.45	4.59	0.02	0.18
MIN 2-2		0.15	1.10	1.00	1.40	1.18	0.11	0.19	0.02	0.65	6.58	0.02	0.25
MIN 7-1		0.05	1.70	1.30	2.81	1.68	0.02	0.22	0.0039	0.13	1.28	0.0048	0.05
MIN 7-2		0.05	1.70	1.15	2.49	1.58	0.02	0.21	0.0042	0.14	1.41	0.0053	0.05
MIN 7-3		n.d.	1.50	0.90	1.72	1.31	n.d.	0.19	n.d.	n.d.	n.d.	n.d.	n.d.
MIN 7-4		n.d.	1.50	1.00	1.91	1.38	n.d.	0.20	n.d.	n.d.	n.d.	n.d.	n.d.

MIN 7-5		n.d.	1.00	0.50	0.64	0.80	n.d.	0.16	n.d.	n.d.	n.d.	n.d.	n.d.
MIN 3-1	Group P2a	n.d.	1.60	0.90	1.83	1.35	n.d.	0.20	n.d.	n.d.	n.d.	n.d.	n.d.
MIN 4-1		n.d.	1.50	0.80	1.53	1.24	n.d.	0.19	n.d.	n.d.	n.d.	n.d.	n.d.
MIN 4-2		n.d.	1.60	1.00	2.04	1.43	n.d.	0.20	n.d.	n.d.	n.d.	n.d.	n.d.
MIN 4-3		n.d.	1.40	1.30	2.32	1.52	n.d.	0.21	n.d.	n.d.	n.d.	n.d.	n.d.
MIN 1-1	Group P2b	n.d.	1.20	0.90	1.38	1.17	n.d.	0.18	n.d.	n.d.	n.d.	n.d.	n.d.
MIN 1-2		n.d.	1.40	1.00	1.78	1.34	n.d.	0.20	n.d.	n.d.	n.d.	n.d.	n.d.
MIN 1-3		n.d.	1.60	1.40	2.85	1.69	n.d.	0.22	n.d.	n.d.	n.d.	n.d.	n.d.
MIN 1-4		n.d.	1.50	1.30	2.48	1.58	n.d.	0.21	n.d.	n.d.	n.d.	n.d.	n.d.
MIN 6-1	Group P3	n.d.	1.70	0.90	1.95	1.40	n.d.	0.20	n.d.	n.d.	n.d.	n.d.	n.d.
MIN 6-2		n.d.	1.70	1.20	2.60	1.61	n.d.	0.21	n.d.	n.d.	n.d.	n.d.	n.d.
MIN 8-1		0.10	1.70	1.50	3.25	1.80	0.03	0.22	0.01	0.22	2.29	0.01	0.09
MIN 8-2		0.45	1.60	1.50	3.06	1.75	0.15	0.22	0.03	1.06	10.79	0.04	0.42
MIN 8-3		0.25	1.50	1.35	2.58	1.61	0.10	0.21	0.02	0.67	6.84	0.03	0.26
MIN 9-1	Group P4a	0.40	1.15	1.10	1.61	1.27	0.25	0.19	0.05	1.55	15.76	0.06	0.61
MIN 10-1		0.80	1.60	1.00	2.04	1.43	0.39	0.20	0.08	2.58	26.27	0.10	1.01
MIN 5-1	Group P4b	0.90	1.30	0.90	1.49	1.22	0.60	0.19	0.11	3.69	37.66	0.14	1.45
MIN 5-2		0.15	0.90	0.30	0.34	0.59	0.44	0.14	0.06	1.92	19.56	0.07	0.75
MIN 11-2	Group C1	n.d.	0.90	0.80	0.92	0.96	n.d.	0.17	n.d.	n.d.	n.d.	n.d.	n.d.
MIN 11-5		n.d.	0.70	0.40	0.36	0.60	n.d.	0.14	n.d.	n.d.	n.d.	n.d.	n.d.
MIN 12-1		n.d.	1.00	0.50	0.64	0.80	n.d.	0.16	n.d.	n.d.	n.d.	n.d.	n.d.
MIN 11-3	Group C2	n.d.	0.80	0.60	0.61	0.78	n.d.	0.15	n.d.	n.d.	n.d.	n.d.	n.d.
MIN 11-4		0.10	1.00	0.80	1.02	1.01	0.10	0.17	0.02	0.55	5.62	0.02	0.22
MIN 11-1	Group C3	n.d.	0.60	0.30	0.23	0.48	n.d.	0.12	n.d.	n.d.	n.d.	n.d.	n.d.
MIN 13-1	Group H	0.15	0.90	0.60	0.69	0.83	0.22	0.16	0.03	1.12	11.43	0.04	0.44
MIN 13-2		0.15	0.80	0.35	0.36	0.60	0.42	0.14	0.06	1.86	19.01	0.07	0.73

P = breaking load; W = width; H = height of specimen; De = equivalent diameter; Is = punching strength index; F = specimen shape factor; $Is_{(50)}$ = punching strength index normalised to a cylindric specimen; R_C = compression strength calculated indirectly; R_T = tensile strength calculated indirectly; n.d. = not determined.

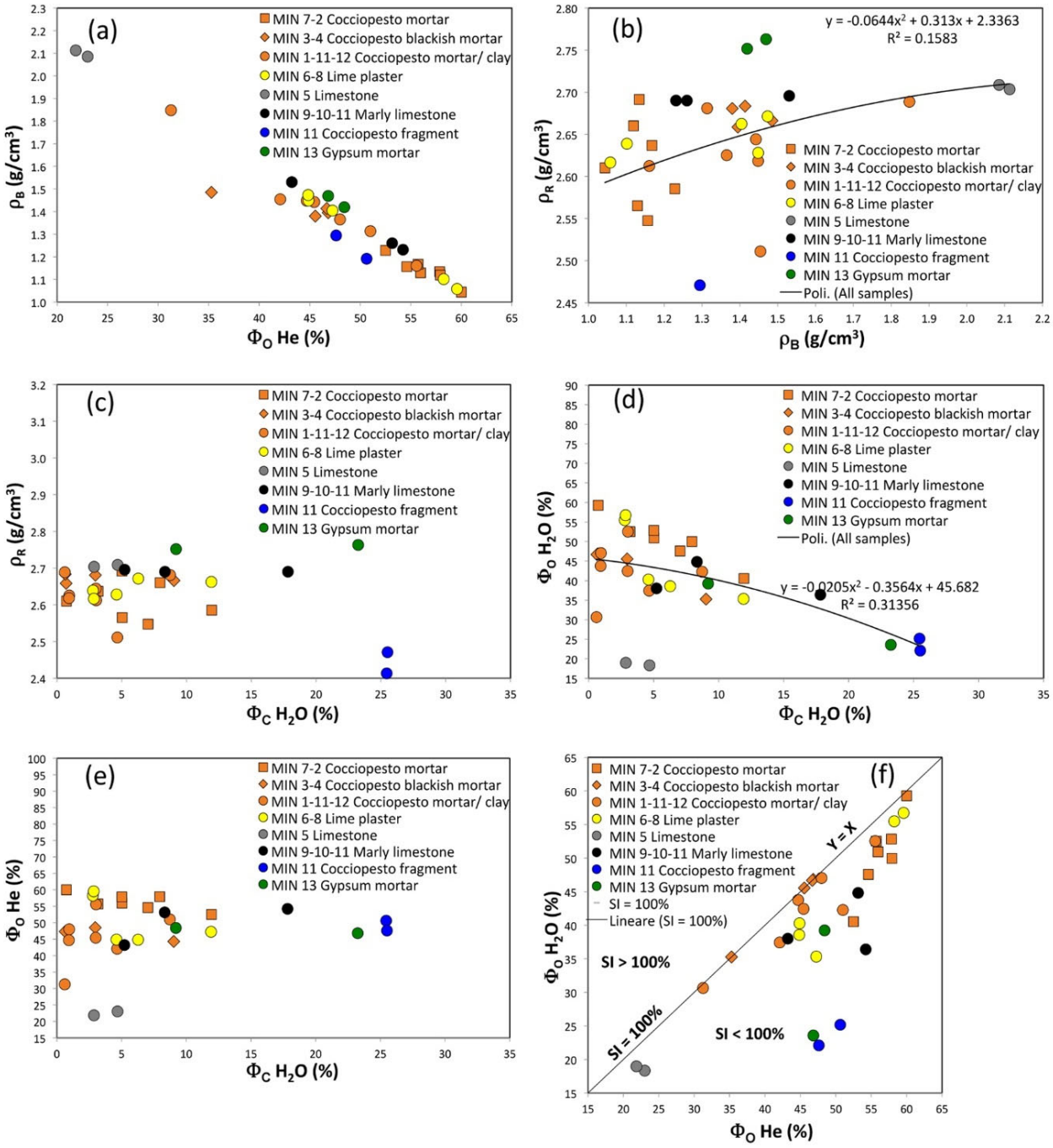

Figure 13. Binary charts which plot the main physical properties of samples taken from Area B and *house-fort* of Cap de Forma archaeological site. (**a**) helium open porosity (Φ_O He) vs. bulk density (ρ_B); (**b**) bulk density (ρ_B) vs. real density (ρ_R); (**c**) water closed porosity (Φ_C H_2O) vs. real density (ρ_R); (**d**) water closed porosity (Φ_C H_2O) vs.—water open porosity (Φ_O H_2O); (**e**) water closed porosity (Φ_C H_2O) vs. helium open porosity (Φ_O He); (**f**) helium open porosity (Φ_O He) vs. water open porosity (Φ_O H_2O).

Figure 13b highlights that the bulk density is affected by porosity and subordinately by real density, with which it shows a (albeit weak) polynomial positive correlation with an R^2 coefficient of 0.16.

The low correlation coefficient is also due to the fact that very different materials are plotted together, such as mortars, lithologies and brick fragments. The variability of the real density (2.41–2.78 g/cm^3, Table 3) is linked to the compositional heterogeneity of the samples; mortar samples, in particular, are characterized by different binder/aggregate ratios and by different mineralogy. The two fragments of cocciopesto show the lower real density values (around 2.4–2.5 g/cm^3) likely due to a matrix poorly interconnected outward, as shown by the high values of closed porosity to water up to 26%. The closed porosity is clearly negatively correlated with the open porosity to water (R^2 = 0.31) while it shows no correlation with the open porosity to helium (Figure 13d).

The saturation index (Table 3) is graphically shown in Figure 13f, reporting the porosity open to helium versus that open to water. The general trend points to lower saturation for the less porous samples. In fact, the samples of the mortars, generally more porous, show values of this index close to the bisector line of 100%, while those of the lithologies and fragments of cocciopesto have values on average lower (Figure 13e, Table 3).

The mechanical strength, determined by the Point Load Test (Table 4), is clearly conditioned by the porosity (Figure 13a) with which it shows a correlation coefficient R^2 of 0.52. Therefore, it is greater in rocks (limestones) than in mortars, which undoubtedly show a higher state of degradation which heavily affects both the porosity and the resistance test. In fact, as can be seen from Table 4, for several samples it was not possible to carry out the test as they were already strongly non-cohesive and partially disintegrated. The incidence of porosity on resistance is also indirectly highlighted by observing graph b of Figure 14, in which a better correlation coefficient R^2 (0.57) is observed between resistance index and bulk density, which is inversely correlated to porosity (see Figure 13a).

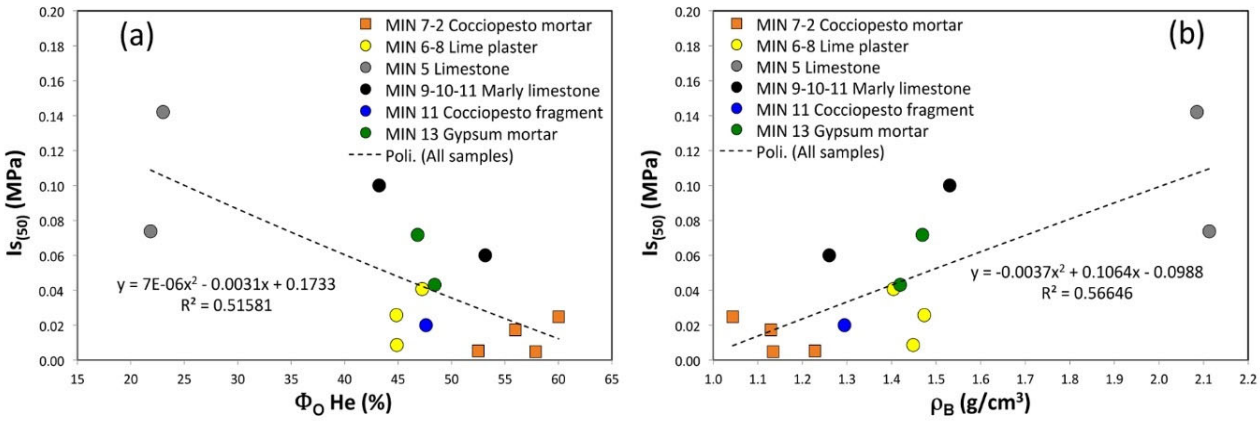

Figure 14. Binary charts which plot the physical-mechanical properties by Point Load Test of samples taken from Area B and *house-fort* of Cap de Forma archaeological site. (**a**) helium open porosity (Φ_O He) vs. punching strength index ($Is_{(50)}$); (**b**) bulk density (ρ_B) vs. punching strength index ($Is_{(50)}$).

6. Discussion

6.1. Function of Mortars and Compositional Features

On the basis of the composition of the aggregate used in mixing with the binder, four main populations of mortars are distinguished:

1. cocciopesto mortars from the pit (groups P1, P2a) with a subordinate fraction of silicate aggregate (e.g., quartz, feldspar, other minor phases) which in some cases shows combustion traces (Group P2);
2. mortars with a cocciopesto aggregate from the pit (subgroups P2b) and from cistern (subgroups C1, C2) with a significant fraction of silicate phases (represented by quartz, feldspars and biotite), and with subordinate clay and particles resulting from combustion adhering to the surface;

3. fine mortars from the pit (group P3) made with a very fine silicate aggregate (substantially of Qtz) in very low percentages (usually <7%) and only in a very subordinate way by small fragments of cocciopesto (probably occasional) and limestone;
4. mortars with a substantially quartz aggregate and subordinate presence of cocciopesto and limestone fragments (group H).

Considering the binder/aggregate ratio and the different aggregate grain size of the mortars described above, it is therefore likely that the sample populations of groups P1, P2a, P2b, H are bedding mortars or plasters (e.g., *arriccio*) or wall or floor covering, while the sample of group P3, considering their low percentage of aggregate, can represent a finishing mortar (*intonachino*).

Based on the binder composition, two main populations are distinguished:

1. mortars (P1, P2a, P2b, P3, C1 groups) with a binder consisting mainly of calcite and pseudo-crystalline-amorphous Ca-carbonatic phases co-precipitated during the carbonation of the binder or secondary phases induced by the alteration of $CaCO_3$;
2. mortars (H group) with a lime and gypsum-based binder, with the presence of bassanite, magnesite and anhydrite deriving from the prolonged drying phase of the samples in the oven (T = 115 °C, during the laboratory preparation of samples) which led to the dehydration of the original plaster.

This different composition is due to the fact that the two types of mortars belong to different historical contexts: the mortar of group H belongs to the 17th –18th century AD since it was sampled in the coeval *house-fort*, while the mortars of P1, P2a, P2b, P3, C1 groups are likely attributable to a Roman phase (see below) even if collected within the area of the first Talaiotic phase (1100–1000 BC).

As regards the carbonate rocks, three main lithologies are distinguished: a fine-grained and porous limestone (subgroup P4a), a weakly marly limestone (?) (subgroup C3) and a more compact limestone (group P4b).

6.2. Materials from the Pit and the Cistern

The mineralogical-petrographic investigations have shown that the mortar samples found inside the pit (US 25), including those interspersed in the US 22 stratigraphic units, and those found in the cistern (US 153, US 154) have a lime-based binder and an aggregate consisting of both a silicate component, mainly represented by quartz and feldspar minerals and cocciopesto with a grain size varying from subcentimetric to millimetric or sometimes submillimetric. In these mortars there are also occasional fragments of local limestone, often of accidental origin deriving from the working process of the limestone. Several pieces of evidence point to a Roman origin of the mortars; firstly, a Talaiotic manufacture can be excluded since this civilization used to build with drystone technique [61]; secondly, the radiocarbon dating on coal frustules inside the mortar indicates the 1st century BC/1st century AD and 3rd and 4th centuries AD ([62] *in press*) consistent with the age of roman occupation [63]; finally, the considerable use of cocciopesto mortars indicates that the materials refer to works of the Roman phase. Moreover, the mortars were correctly used as a lining of the cistern (which originally contained water) to make the internal walls and especially the bottom waterproof suggesting the know-how typical of Romans. The cistern, already used in the Talaiotic phase, presents clear fractures in the rocky substrate that would not have allowed good waterproofing. However, the sealing intervention seems to be not efficient. The low reactivity between the cocciopesto fragments and the lime-binder, quite evident despite the significant degradation, lead to the development of a feebly hydraulic mortar. We can just hypothesize the reason of this low reactivity that could be due to the high content of quartz and feldspars, highlighted by the petrographic analyses, and/or to the low firing temperature resulting in low sintering degree. These features contrast with the evolved production technologies of Romans in that period [64,65]. Thus, it could be argued that cocciopesto fragments derive from low-quality local pottery referable to the Talaiotic I period that is the most abundant in the site [66].

These ceramics were fired at low temperature and abundant carbonate fractions were added to the paste to lower the melting point [44]. On the other hand, very low quartz and feldspar contents are detected in the exact same ceramics [44], thus contrasting with our findings. Further analyses are thus required to clarify this interesting topic.

As regards the binder, petrographic and XRD analyses revealed the presence of several phases beyond the more obvious calcite. The presence in ancient Roman mortars of aragonite, a metastable polymorph of calcite, is known in literature [21] and can be justified by assuming the presence of marine fossils with carbonate composition in the aggregate fragments or by dissolution and subsequent recrystallization of the same calcitic binder [67]. The dolomite [$CaMg(CO_3)_2$], present in traces, probably derives from the calcareous rock used for the production of lime or from the aggregate. This is a reasonable assumption since the surrounding outcrops of limestone, the most likely source of raw materials for lime production and occasionally for aggregate's supply, are widely dolomitized [55]. It is worth noting that dolomite, Mg-rich calcite and aragonite have been found also in mortars from the nearby roman city of Pollentia (Mallorca) [68].

The presence of periclase (MgO) is quite interesting. The more obvious geologic source of Mg in the surrounding area is the dolomitic limestone [55] and it is well known that between 700 and 800 °C, it decomposes according to the reaction [69]:

$$CaMg(CO_3)_2 \Rightarrow CaCO_3 + MgO + CO_2$$

and possible subsequent reaction:

$$CaCO_3 \Rightarrow CaO + CO_2$$

So, burning the local limestone for lime production would easily produce periclase. Interestingly, brucite $Mg(OH)_2$ that is the hydrated counterpart of periclase was also found in the cocciopesto fragments from Talaiotic pottery from Cap de Forma [44]; thus, our finding by XRD could be also linked to its presence in the cocciopesto rather than in the binder. Although periclase under atmospheric conditions tends to hydrate forming brucite [$Mg(OH)_2$], its presence is not uncommon in ancient, and thus aged, mortars [70]. Different causes can hinder the periclase hydration, such as the burning temperature, the slaking method, the particle grain size, the climate conditions, etc. [71,72].

Physical analyses revealed a high open porosity of the mortars, also characterized by a high variability (31–60%), with consequent low values of apparent density (ranging from 1.85 to 1.04 g/cm^3, respectively). Such high porosity values cannot be referred solely to technical defect during their production but also the severe chemical-physical decay that the mortars have undergone over the course of about two millennia. The binder has undergone a significant weathering due to $CaCO_3$ dissolution processes and also, given its proximity to the sea, due to marine aerosol. The cyclical mechanism of precipitation/solubilisation of the high solubility saline phases in fact involves a strong crystallization pressure inside the porosity of the material with an important disintegrating physical action [73,74]. As highlighted by the Point Load Test, the mortars have a poor mechanical competence, which can be explained by the high porosity and by the low hydraulic degree of the carbonate binder.

Considering the coarse grain size of aggregates observed in some samples, it could be hypothesized that in some cases they had a function of bedding mortars between ashlars. However, the low mechanical resistance and the high binder/aggregate ratios determined on a microscopic scale suggest that the analysed mortars may have had a function as simple plaster of the masonry or wedging mortars. However, considering that: (i) the binder/aggregate ratios on a macroscopic basis are actually lower (conceivable 1: 1 and in some cases 1: 2) than those determined by IA-OM, (ii) the compositional and grain size heterogeneity of the aggregate used, (iii) the frequent presence of "incotti" (i.e., un-/underfired limestone fragments) and lime lumps indicating a rough treatment of limestone (or calcarenite) used for the binder production, more likely, it is conceivable that such mortars (or at least a part of them) have been used mainly to create the floors or to a limited extent

also for the wall cladding of the cisterns. These floors were probably made preparing a first (innermost) layer, consisting of a compacted clayey layer, on which the lime-based mortar was spread. In support of this hypothesis, there are some other important technical-constructive pieces of evidence:

1. laying of the various mortar samples on a poorly- to well-compacted clay layer, referable to the substrate of the flooring or of the wall underlying the mortar;
2. presence of fine-grained mortar samples with a very high binder/aggregate ratio (95/5%), probably referable to the external finishing layer;
3. poor resistance of the mortars which would not have had good physical-mechanical characteristics to withstand the loads of the imposing stone walls.

As regards the lithologies, the mineralogical-petrographic analyses of the rock samples have highlighted the use of local lithofacies, easily available on site, both for the construction of the walls and for the occasional use as aggregate in mortars. These geomaterials are generally more resistant than mortars even though they show very low mechanical resistance values in absolute terms compared to "fresh" rocks, indicating that degradation severely affected their resistance.

6.3. Mortars from the House-Fort

The results of the mineralogical-petrographic analyses on the few samples found in the Cap de Forma *house-fort* showed the use, in this specific case, of a mortar with a gypsum-based binder. XRD analyses show the predominance of bassanite and anhydrite, both referable to the partial or total dehydration of the gypsum, respectively, and a subordinate presence of calcite. Aggregates consist of a silicate fraction (mainly represented by quartz) and only occasionally fragments of local dolomites, as evidenced by the XRD analyses which highlighted the presence of dolomite and magnesite. Cocciopesto, on the contrary, is totally absent. The possibility that gypsum derives from sulfation processes of the carbonate binder seems to be unlikely. Indeed, even though gypsum can form in lime mortars interacting with marine-aerosol [73], in this case gypsum is too abundant and carbonates too scarce to hypothesize such an origin. The reason why calcium sulphate is found in the two hemihydrate and anhydrous forms instead of the di-hydrated one (gypsum, $CaSO_4 \bullet 2H_2O$) is likely linked to the sample preparation since dehydration can easily occur both during drying and grinding gypsum-rich samples [75].

The low particle size of the aggregate (usually submillimetric) and a binder/aggregate ratio of about 70/30, suggest that this mortar had a plaster function. Considering that the sample was found inside a stratigraphic unit (US 134) which can be interpreted as the layer pertaining to the collapse of the upper parts and the roof of the building, the plaster could derive from the walls, whose surfaces still retain small fragments in place but also it cannot be ruled out that it comes from the internal ceiling. The presence of a geometric texture on the external surface of the mortar sample (Figure 15) was probably left by a panel of weaved reed fibres (perhaps positioned below and "on sight"), supporting the latter hypothesis. Considering the historical period (17^{th}–18^{th} centuries), in which the massive use of hydraulic lime was not yet developed [76,77], the use of mortars with a mixed base of lime and gypsum was not uncommon.

Figure 15. Lime/gypsum mortar taken from *house-fort* of Cap de Forma. Detail of geometric texture on the external surface of the sample, probably made with an intertwining of reed fibres (reed, perhaps positioned below and "visible").

Unlike mortars based on lime and cocciopesto, in this case the binder based on lime and gypsum is more coherent and more competent from a mechanical point of view. The resistance to punching is higher than the degraded mortars based on lime and cocciopesto. This is explained by a lower open porosity of these gypsum mortars (24–39%), resulting in lower bulk density values (1.42–1.47 g/cm^3) and higher values of the real density (2.75–2.76 g/cm^3) explained by the presence of bassanite (2.73 g/cm^3) and above all dolomite (2.84 g/cm^3) and magnesite (2.98 g/cm^3). The porosity values are in any case quite high and even in this case it is possible that the degradation induced by the marine aerosol and the constant daily hygrometric variations (given the proximity of the sea) have led to a chemical-physical alteration of the lime-gypsum binder, although it was mainly concentrated on its surface of mortar.

6.4. Provenance of Raw Materials

Mortars are complex materials resulting from the mixing of different components and from thermal and chemical transformation, thus defining the provenance of raw materials is commonly complicated and requires a multidisciplinary and multi-instrumental approach ([78] and references therein, [13]). In the case of Cap de Forma archaeological site, this kind of study is probably simplified by the insularity and thus by the geographical barriers that make it difficult to import raw materials from sites other than the island itself.

So, even without a specific analytical approach, some reliable consideration can be done. Based on the here presented data, four main raw materials can be identified: limestone for lime binder, silicate minerals and cocciopesto necessary and aggregate of Roman mortars and gypsum used in the more recent plasters. The supply of limestones was obviously not difficult since it is widespread in the whole southern sector of Menorca Island. Even lacking a precise identification of limestone quarries, we can reasonably hypothesise a local source not so far from the archaeological site. This assumption is further confirmed by chemical analyses performed by SEM-EDS that revealed an almost ubiquitous presence of magnesium in the binder (authors' unpublished data) and by XRPD analyses that detected the peaks of dolomite in several samples. Indeed, it is well documented that local

limestones are partly to totally dolomitised, thus explaining the source of magnesium found in the mortars.

Cocciopesto provenance has been already discussed (see above). The low quality of ceramics, likely produced by low temperature firing and maybe with an inadequate material selection, supports a non-Roman manufacturing. We can just speculate about their origin from Talaiotic culture, but this hypothesis should be constrained by more detailed analyses and by the comparison between known Talaiotic pottery findings and the cocciopesto fragments found within the mortars.

The provenance of silicate aggregates should also be explained. Commonly, the supply of quartz and feldspars sand is quite easy since these are among the most common minerals worldwide occurring in the most diverse geological environments. The Cap de Forma case study represents an exception since quartz and feldspar, in variable amounts, can be found in the surrounding area but are commonly cemented by limestone and/or dolostone to form the Upper Miocene carbonate succession of the southern island [55]. Loose quartz/feldspathic sediment, to be used as an aggregate, could be found in beaches or in streambeds. However, the mineralogical composition of the sands from the beaches in the area of Cap de Forma is dominated by biogenic and fossiliferous materials [79] not compatible with the aggregates found in the mortars. Interestingly, a marked quartz-rich, terrigenous content is found in beach sediments from the central sector of the southern coast [79] at about 15 km northwest from the Cap de Forma site. Lacking data on the streambed sediment compositions in the study area, it is not possible to assess a possible provenance of these materials, but this oddity can be a starting point for further investigations.

As regards gypsum-based mortars, their use in Spanish territory during the historical period is well known in the literature [80,81]. Its use is concentrated mainly between the 18th and 19th centuries, and only in a subordinate form at the beginning of the 20th century, gradually disappearing due to the increasing presence of other more recent binders, including cement. An interesting example is the use of gypsum mortars on historical facades in the centre of Valencia, which represents a particular aspect of the city's building tradition and confirms the existence of a specific ancient technique in the use of gypsum linked to the type of building, the style of the facade and the historical period [82]. Therefore, based on these considerations, it is possible to assume that the mortars found in the *house-fort* belong to the late 18th century. The supply of the raw gypsum for binder production is an open question. The presence of sulphate-evaporitic rock quarries in the Menorca Island is not documented in the bibliography, whereas some occurrences from the nearby island of Mallorca are reported [83,84]. The age of the first gypsum exploitation is documented at the end of 17th century by the appearance of toponyms containing the word "*guix*" (= gypsum in Catalan language) in the northern Mallorca [83]. Interestingly, also in the central-north coast of Menorca Island, toponyms like "*baix des guix*" (gypsum bay) and "*clot des guix*" (gypsum lump) can be found; this could indicate either a local supply point (not visible now) or a port used to dock ships carrying gypsum.

7. Conclusions

This research made it possible to define the compositional characteristics and the physical-mechanical properties of the construction materials (mortars, stones) found in the archaeological site of Cap de Forma. These materials were used in the construction of ancient structures that are now degraded and remodelled, of which today we can only observe the ruins of the structures.

The comparison of the compositional aspects of the materials, reflecting different construction technologies, was performed taking into account the historical contexts and the civilization phases that followed one another in time (Talaiotic period, Roman phase, recent constructions of the 17th–18th century).

The results show that:

- Mortars were not used in the constructions of the Talaiotic phase as highlighted, for instance, by the water cistern, whose sealing by plastering occurred in later times;
- The use of mortars to seal the cistern occurred during the Roman phase as testified by cocciopesto aggregates and further confirmed by radiocarbon dating carried out on charcoal frustules inside two cocciopesto-mortars found at the bottom of the cistern, that date the materials at 1st century BC—4th century AD ([62], *in press*);
- Two kinds of mortars, one with a coarse aggregate, another with a finer aggregate, were found. The coarser one, called Rudus, was used in contact with the rock as indicated by soil adhering to the samples); the finer one rich in cocciopesto was a kind of finishing plaster;
- The strong decay of these mortars is largely due to the weathering but indicates also a low hydraulicity of mortars and thus a low reactivity of cocciopesto. This led us to make some hypotheses on the provenance of pottery used to produce cocciopesto that are worth being further investigated.
- The mortars from the *house-fort* are significantly different from those from the cistern, being gypsum based. By checking the literature, it is found that gypsum was widely used for plastering in the period of the *house-fort* settlement (17th–18th century) in different parts of Spain and that a local source of raw materials is found in the nearby Mallorca Island.

Author Contributions: Conceptualization, S.C. and A.D.; methodology, S.C. and D.F.; validation, A.D. and G.G.; formal analysis, D.F. and G.B.; investigation, A.D., G.B. and D.F.; resources, S.C.; data curation, S.C. and D.F.; writing—original draft preparation, S.C.; writing—review and editing, D.F. and S.C.; visualization, D.F. and S.C.; supervision, S.C.; project administration, S.C.; funding acquisition, S.C. All authors have read and agreed to the published version of the manuscript.

Acknowledgments: We thank Vincenzina La Spina of Departamento de Arquitectura y Tecnología de la Edificación, Grupo de Historia de la Construcción (Universidad Politécnica de Cartagena) for historical-architectural data on the Spanish ancient gypsum mortars and CeSAR (Centro Servizi d'Ateneo per la Ricerca, Cittadella Universitaria, 09042 Monserrato, Cagliari University) for willingness to use the electron microscope (SEM).

Conflicts of Interest: The authors declare no conflict of interest.

References

1. Karner, D.B.; Lombardi, L.; Marra, F.; Fortini, P.; Renne, P.R. Age of ancient monuments by means of building stone provenance: A case study of the Tullianum, Rome, Italy. *J. Archaeol. Sci.* **2001**, *28*, 387–393.
2. Columbu, S.; Antonelli, F.; Lezzerini, M.; Miriello, D.; Adembri, B.; Blanco, A. Provenance of marbles used in the Heliocaminus Baths of Hadrian's Villa (Tivoli, Italy). *J. Archaeol. Sci.* **2014**, *49*, 332–342, https://doi.org/10.1016/j.jas.2014.05.026.
3. Columbu, S.; Gaviano, E.; Costamagna, L.G.; Fancello, D. Mineralogical-petrographic and physical-mechanical features of the construction stones in Punic and Roman temples of Antas (SW Sardinia, Italy): Provenance of the raw materials and conservation state. *Minerals* **2021**, *11*, 964, https://doi.org/10.3390/min11090964.
4. Montana, G. Ceramic raw materials. In *The Oxford Handbook of Archaeological Ceramic Analysis*; Hunt, A.M. Ed.; Oxford University Press: Oxford, UK, 2017; pp. 87–100.
5. Hein, A.; Kilikoglou, V. Ceramic raw materials: How to recognize them and locate the supply basins: Chemistry. *Archaeol. Anthropol. Sci*. **2020**, *12*, 1–17.
6. Ortega, L.A.; Zuluaga, M.C.; Alonso-Olazabal, A.; Murelaga, X.; Alday, A. Petrographic and geochemical evidence for long-standing supply of raw materials in neolithic pottery (Mendandia site, Spain). *Archaeometry* **2010**, *52*, 987–1001.
7. Henderson, J. The raw materials of early glass production. *Oxf. J. Archaeol.* **1985**, *4*, 267–291.
8. Degryse, P.; Schneider, J. Pliny the Elder and Sr–Nd isotopes: Tracing the provenance of raw materials for Roman glass production. *J. Archaeol. Sci*. **2008**, *35*, 1993–2000.
9. Brems, D.; Degryse, P.; Hasendoncks, F.; Gimeno, D.; Silvestri, A.; Vassilieva, E.; Luypaers, E.; Honings, J. Western Mediterranean sand deposits as a raw material for Roman glass production. *J. Archaeol. Sci.* **2012**, *39*, 2897–2907.
10. Columbu, S.; Garau, A.M.; Lugliè, C. Geochemical characterisation of pozzolanic obsidian glasses used in the ancient mortars of Nora Roman theatre (Sardinia, Italy): Provenance of raw materials and historical–archaeological implications. *Archaeol. Anthropol. Sci.* **2019**, *11*, 2121–2150, https://doi.org/10.1007/s12520-018-0658-y.

11. Columbu, S.; Sitzia, F.; Ennas, G. The ancient pozzolanic mortars and concretes of Heliocaminus baths in Hadrian's Villa (Tivoli, Italy). *Archaeol. Anthropol. Sci.* **2017**, *9*, 523–553, https://doi.org/10.1007/s12520-016-0385-1.
12. Falkenberg, J.; Mutterlose, J.; Kaplan, U. Calcareous nannofossils in medieval mortar and mortar-based materials: A powerful tool for provenance analysis. *Archaeometry* **2021**, *63*, 19–39.
13. Ortega, L.A.; Zuluaga, M.C.; Alonso-Olazabal, A.; Insausti, M.; Ibañez, A. Geochemical characterization of archaeological lime mortars: Provenance inputs. *Archaeometry* **2008**, *50*, 387–408.
14. Elsen, J.; Mertens, G.; Van Balen, K. Raw materials used in ancient mortars from the Cathedral of Notre-Dame in Tournai (Belgium). *Eur. J. Mineral.* **2011**, *23*, 871–882.
15. Columbu, S.; Garau, A.M. Mineralogical, petrographic and chemical analysis of geomaterials used in the mortars of Roman Nora theatre (south Sardinia, Italy). *Ital. J. Geosci.* **2017**, *136*, 238–262, https://doi.org/10.3301/IJG.2017.05.
16. Acquafredda, P.; Muntoni, I.M. Obsidian from Pulo di Molfetta (Bari, Southern Italy): Provenance from Lipari and first recognition of a Neolithic sample from Monte Arci (Sardinia). *J. Archaeol. Sci.* **2008**, *35*, 947–955.
17. Belfiore, C.M.; Ricca, M.; La Russa, M.F.; Ruffolo, S.A.; Galli, G.; Barca, D.; Malagodi, M.; Vallefuoco, M.; Sprovieri, M.; Pezzino, A. Provenance study of building and statuary marbles from the Roman archaeological site of "Villa dei Quintili" (Rome, Italy). *Ital. J. Geosci.* **2016**, *135*, 236–249.
18. Columbu, S. Petrographic and geochemical investigations on the volcanic rocks used in the Punic-Roman archaeological site of Nora (Sardinia, Italy*). Environ. Earth Sci.* **2018**, *77*, 577, https://doi.org/10.1007/s12665-018-7744-4.
19. DeLaine, J. Production, transport and on-site organisation of Roman mortars and plasters. *Archaeol. Anthropol. Sci.* **2021**, *13*, 1–17.
20. Schiavon, N.; Mazzocchin, G.A. The provenance of sand in mortars from Roman villas in NE Italy: A chemical–mineralogical approach. *Open Mineral. J.* **2009**, *3*, 32–39.
21. Borsoi, G.; Silva, A.S.; Menezes, P.; Candeias, A.; Mirão, J.A.P. Analytical Characterization of Ancient Mortars from the Archaeological Roman Site of Pisões (Beja, Portugal). *Constr. Build. Mater.* **2019**, *204*, 597–608.
22. Columbu, S.; Lisci, C.; Sitzia, F.; Lorenzetti, G.; Lezzerini, M.; Pagnotta, S.; Raneri, S.; Legnaioli, S.; Palleschi, V.; Gallello, G.; et al. Mineralogical, petrographic and physical-mechanical study of Roman construction materials from the Maritime Theatre of Hadrian's Villa (Rome, Italy). *Measurement* **2018**, *127*, 264–276, https://doi.org/10.1016/j.measurement.2018.05.103.
23. Rispoli, C.; De Bonis, A.; Esposito, R.; Graziano, S.F.; Langella, A.; Mercurio, M.; Morra, V.; Cappelletti, P. Unveiling the secrets of roman craftsmanship: Mortars from Piscina Mirabilis (Campi Flegrei, Italy). *Archaeol. Anthropol. Sci.* **2020**, *12*, 2–18, https://doi.org/10.1007/s12520-019-00964-8.
24. Columbu, S.; Palomba, M.; Sitzia, F.; Murgia, M.R. Geochemical, mineral-petrographic and physical-mechanical characterisation of stones and mortars from the Romanesque Saccargia Basilica (Sardinia, Italy) to define their origin and alteration. *Ital. J. Geosci.* **2018**, *137*, 369–395, https://doi.org/10.3301/IJG.2018.04.
25. Marra, F.; D'Ambrosio, E.; Gaeta, M.; Mattei, M. Petrochemical identification and insights on chronological employment of the volcanic aggregates used in ancient Roman mortars. *Archaeometry* **2016**, *58*, 177–200.
26. Nawrocka, D.; Michniewicz, J.; Pawlyta, J.; Pazdur, A. Application of radiocarbon method for dating of lime mortars. *Geochronometria* **2005**, *24*, 109–115.
27. Pavía, S.; Caro, S. An investigation of Roman mortar technology through the petrographic analysis of archaeological material. *Constr. Build. Mat.* **2008**, *22*, 1807–1811.
28. Ramacciotti, M.; Rubio, S.; Gallello, G.; Lezzerini, M.; Columbu, S.; Hernandez, E.; Morales-Rubio, A.; Pastor, A.; De La Guardia, M. Chronological classification of ancient mortars employing spectroscopy and spectrometry techniques: Sagunto (Valencia, Spain) Case. *J. Spectrosc.* **2018**, *2018*, 9736547, https://doi.org/10.1155/2018/9736547.
29. Sitzia, F. (2021). The San Saturnino Basilica (Cagliari, Italy): An Up-Close Investigation about the Archaeological Stratigraphy of Mortars from the Roman to the Middle Ages. *Heritage* **2021**, *4*, 1836–1853.
30. Waelkens, M.; Herz, N.; Moens, L. *Ancient Stones: Quarrying, trade and provenance: Interdisciplinary studies on stones and stone technology in Europe and near East from the Prehistoric to the Early Christian Period (No. 4);* Leuven University Press: Leuven, Belgium, 1992; ISBN 978-9061864943.
31. Columbu, S.; Palomba, M.; Sitzia, F.; Carcangiu, G.; Meloni, P. Pyroclastic Stones as Building Materials in Medieval Romanesque Architecture of Sardinia (Italy): Chemical-Physical Features of Rocks and Associated Alterations. *Int. J. Archit. Herit.* **2022**, *16*, 49-66, https://doi.org/10.1080/15583058.2020.1749729.
32. Moropoulou, A.; Polikreti, K.; Bakolas, A.; Michailidis, P. Correlation of physicochemical and mechanical properties of historical mortars and classification by multivariate statistics. *Cem. Concr. Res.* **2020**, *33*, 891–898.
33. Columbu, S.; Gioncada, A.; Lezzerini, M.; Sitzia, F. Mineralogical-chemical alteration and origin of ignimbritic stones used in the old Cathedral of Nostra Signora di Castro (Sardinia, Italy). *Stud. Conserv.* **2019**, *64*, 397–422, https://doi.org/10.1080/00393630.2018.1565016, WOS:000463289900001.
34. Aragoni, M.C.; Giacopetti, L.; Arca, M.; Carcangiu, G.; Columbu, S.; Gimeno, D.; Isaia, F.; Lippolis, V.; Meloni, P.; Ezquerra, A.N.; et al. Ammonium monoethyloxalate (AmEtOx): A new agent for the conservation of carbonate stone substrates. *New J. Chem.* **2021**, *45*, 5327–5339.
35. Sitzia, F.; Beltrame, M.; Columbu, S.; Lisci, C.; Miguel, C.; Mirão, J. Ancient restoration and production technologies of Roman mortars from monuments placed in hydrogeological risk areas: A case study. *Archaeol. Anthropol. Sci.* **2020**, *12*, 147.

36. Degryse, P.; Elsen, J.; Waelkens, M. Study of ancient mortars from Sagalassos (Turkey) in view of their conservation. *Cem. Concr. Res.* **2002**, *32*, 1457–1463.
37. Morricone, A.; Macchia, A.; Campanella, L.; David, M.; de Togni, S.; Turci, M.; Maras, A.; Meucci, C.; Ronca, S. Archeometrical analysis for the characterization of mortars from Ostia Antica. *Procedia Chem.* **2013**, *8*, 231–238.
38. Columbu, S. Provenance and alteration of pyroclastic rocks from the Romanesque Churches of Logudoro (north Sardinia, Italy) using a petrographic and geochemical statistical approach. *Appl. Phys. A Mater. Sci. Process.* **2017**, *123*, 165, https://doi.org/10.1007/s00339-017-0790-z.
39. Vola, G.; Gotti, E.; Brandon, C.; Oleson, J.P.; Hohlfelder, R.L. Chemical, mineralogical and petrographic characterization of roman ancient hydraulic concretes cores from Santa Liberata, Italy, and Caesarea Palestinae, Israel. *Period. Miner.* **2011**, *80*, 317–338.
40. Antonelli, F.; Columbu, S.; Lezzerini, M.; Miriello, D. Petrographic characterisation and provenance determination of the white marbles used in the roman sculptures of Forum Sempronii (Fossombrone, Marche, Italy). *Appl. Phys. A Mater. Sci. Process.* **2014**, *115*, 1033–1040, https://doi.org/10.1007/s00339-013-7938-2.
41. Antonelli, F.; Columbu, S.; De Vos Raaijmakers, M.; Andreoli, M. An archaeometric contribution to the study of ancient millstones from the Mulargia area (Sardinia, Italy) through new analytical data on volcanic raw material and archaeological items from Hellenistic and Roman North Africa. *J. Archaeol. Sci.* **2014**, *50*, 243–261, https://doi.org/10.1016/j.jas.2014.06.016.
42. Depalmas, A. New data from fortified coastal settlement of Cap de Forma, Mahon, Menorca (Balearic Islands). *Radiocarbon* **2014**, *56*, 425–437.
43. Lagarda Mata, F. *Menorca Talayótica*; Lagarda Mata, F. Ed.; Alfajarin, Spain, 2015; ISBN: 978-84-96810-41-9.
44. Plantalamor Massanet, L.; Tanda, G.; Tore, G.; Baldaccini, P.; Del Vais, C.; Depalmas, A.; Marras, G.; Mameli, P.; Mulé, P.; Oggiano, G.; et al. Cap de Forma (Minorca): La navigazione nel Mediterraneo occidentale dall'età del bronzo all'età del ferro. Nota preliminare. In *Antichità Sarde. Studi e Ricerche 5*; Tanda, G. Ed; Stamperia Artistica; Università di Sassari: Sassari, Italy, 1999; pp. 11–160.
45. SEGUÍ, T. Las excavaciones de Cap de Forma descubren una cisterna talayótica. Menorca.info. Maó: Editorial Menorca S.A., Spain, 2011. Edición electrónica en:.
Available online: https://www.menorca.info/menorca/local/2011/06/26/1404306/excavaciones-cap-forma-descubren-cisterna-talayotica.html (accessed on 23 December 2021)
46. Depalmas, A.; Columbu, S. . In: *Modern Age Fortifications of the Mediterranean Coast–Defensive Architecture of the Mediterranean: XV to XVIII Centuries (Fortmed 2015)*; Editorial Universitat Politècnica de València, Ed.; Editorial Universitat Politècnica de València, Spain, 2015; Volume II, pp. 381–388.
47. Escudero-Mozo, M.J.; Martín-Chivelet, J.; Goy, A.; López-Gómez, J. Middle-Upper Triassic carbonate platforms in Minorca (Balearic Islands): Implications for Western Tethys correlations. *Sediment. Geol.* **2014**, *310*, 41–58.
48. Carminati, E.; Wortel, M.J.R.; Spakman, W.; Sabadini, R. The role of slab detachment processes in the opening of the western–central Mediterranean basins: Some geological and geophysical evidence. *Earth Planet. Sc. Lett.* **1998**, 160, 651–665.
49. Sàbat, F.; Gelabert, B.; Rodriguez-Perea, A.R. Minorca, an exotic Balearic island (western Mediterranean). *Geol. Acta* **2018**, *16*, 411–426.
50. Rosell, J.; Elízaga, E. Evolución tectosedimentaria del Paleozoico de la isla de Menorca. *Bol. Geol. Min.* **1989**, *100*, 193–204.
51. Elízaga, E.; Rosell, J.; Gómez, D. Mapa Geológico de la Isla de Menorca a escala 1:100.000. Cartografía geológica regional, **1992**. ©Instituto Geológico y Minero de España (IGME). Available online: http://info.igme.es/cartografiadigital/geologica/mapa.aspx?parent=../geologica/geologiaregional.aspx&Id=2&language=es (accessed on 23 December 2021).
52. Linol, B.; Bercovici, A.; Bourquin, S.; Diez, J.B.; López-Gómez, J.; Broutin, J.; Durand, M.; Villanueva-Amadoz, U. Late Permian to Middle Triassic correlations and palaeogeographical reconstructions in south-western European basins: New sedimentological data from Minorca (Balearic Islands, Spain). *Sediment. Geol.* **2009**, 220, 77–94.
53. Fornós, J.J.; Pomar, L.; Ramos-Guerrero, E. Balearic Islands. In *The Geology of Spain*; Gibbons, W., Moreno, T. Eds., The Geological Society: London, UK, 2002; pp. 327–334.
54. Obrador, A.; Pomar, L.; Rodriguez, A.; Jurado, M.J. Unidades deposicionales del Neógeno menorquín. *Acta Geol. Hispán.* **1983** 18(2), 87–97.
55. Pomar, L.; Obrador, A.; Westphal, H. Sub-wavebase cross-bedded grainstones on a distally steepened carbonate ramp, Upper Miocene, Menorca, Spain. *Sedimentology* **2002**, *49*, 139–169.
56. Columbu, S.; Mulas, M.; Mundula, F.; Cioni, R. Strategies for helium pycnometry density measurements of welded ignimbritic rocks. *Meas. J. Int. Meas. Confed.* **2021**, *173*, 108640.
57. Columbu, S.; Cruciani, G.; Fancello, D.; Franceschelli, M.; Musumeci, G. Petrophysical properties of a granite-protomylonite-ultramylonite sequence: Insight from the Monte Grighini shear zone, central Sardinia, Italy. *Eur. J. Mineral.* **2014**, *27*, 471–486, https://doi.org/10.1127/ejm/2015/0027-2447.
58. ISRM-Int. Society for Rock Mechanics and Rock Engineering. Suggested method for determining the point load strength index. In *International Society for Rock Mechanics*; Document 1: 8–12; Committee on Field Tests, ISRM: Lisbon, Portugal, 1972.
59. ISRM-International Society for Rock Mechanics and Rock Engineering. Suggested method for determining the point load strength. In *International Society for Rock Mechanics*; Abstr 22: 51–60; ISRM Commission for Testing Methods, Working Group on Revision of the Point Load Test Methods, ISRM: Lisbon, Portugal, 1985.

60. Roduit, N. JMicroVision: Image analysis toolbox for measuring and quantifying components of high-definition images. Version 1.3.3. Available online: https://jmicrovision.github.io (accessed on 6 June 2020).
61. Anglada, M.; Ferrer, A.; Plantalamor, L.; Ramis, D.; Van Strydonck, M.; De Mulder, G. Chronological framework for the early Talayotic period in Menorca: The settlement of Cornia Nou. *Radiocarbon* **2014**, *56*, 411–424.
62. Depalmas, A. Cap de Forma–Maó. Un asentamiento costero de la Edad del Bronce, in press, Pub.: Aracne, Roma.
63. Ranieri, G.; Godio, A.; Loddo, F.; Stocco, S.; Casas, A.; Capizzi, P.; Messina, P.; Orfila, M.; Cau, M.A.; Chávez, M.E. Geophysical prospection of the Roman city of Pollentia, Alcúdia (Mallorca, Balearic Islands, Spain). *J. Appl. Geophys.* **2016**, *134*, 125–135.
64. Lund, J. *A Study of the Circulation of Ceramics in Cyprus from the 3rd Century BC to the 3rd Century AD*; Aarhus University Press: Aarhus, Denmark, 2015; ISBN 978 87 7124 450 2.
65. Freestone, I.C.; Rigby, V. The introduction of Roman ceramic styles and techniques into Roman Britain: A case study from the King Harry Lane Cemetery, St. Albans, Hertfordshire. In *MRS Online Proceedings Library Archive*; Cambridge University Press: Cambridge, UK, 1988; Volume 123.
66. Plantalamor Massanet, Ll. L'arquitectura prehistòrica i protohistòrica de Menorca i el seu marc cultural. Ph.D. Thesis, Universitat de Barcelona, Barcelona, Spain, 1991.
67. Silva, A.S.; Cruz, T.; Paiva, M.J.; Candeias, A.; Adriano, P.; Schiavon, N.; Mirão, J.A.P. Mineralogical and chemical characterization of historical mortars from military fortifications in Lisbon harbour (Portugal). *Environ. Earth Sci.* **2011**, *63*, 1641–1650.
68. De Luca, R.; Ontiveros, M.C.; Miriello, D.; Pecci, A.; Le Pera, E.; Bloise, A.; Crisci, G.M. Archaeometric study of mortars and plasters from the Roman City of Pollentia (Mallorca-Balearic Islands). *Period. Mineral.* **2013**, *82*, 353–379.
69. Gunasekaran, S.; Anbalagan, G. Thermal decomposition of natural dolomite. *Bull. Mat. Sci.* **2007**, *30*, 339–344.
70. Artioli, G.; Secco, M.; Addis, A. The Vitruvian legacy: Mortars and binders before and after the Roman world. *EMU Notes Miner.* **2019**, *20*, 151–202.
71. Aphane, M.E. The hydration of magnesium oxide with different reactivities by water and magnesium acetate. Master's Thesis, University of South Africa, Pretoria, South Africa, 2007.
72. Rosell, J.R.; Haurie, L.; Navarro, A.; Cantalapiedra, I.R. Influence of the traditional slaking process on the lime putty characteristics. *Constr. Build. Mater.* **2014**, *55*, 423–430.
73. Maravelaki-Kalaitzaki, P.; Bakolas, A.; Moropoulou, A. Physico-chemical study of Cretan ancient mortars. *Cem. Concr. Res.* **2003**, *33*, 651–661.
74. Vallet, J.M.; Gosselin, C.; Bromblet, P.; Rolland, O.; Vergès-Belmin, V.; Kloppmann, W. Origin of salts in stone monument degradation using sulphur and oxygen isotopes: First results of the Bourges cathedral (France). *J. Geochem. Expl.* **2006**, 88, 358–362.
75. Herrero, J.; Artieda, O.; Hudnall, W.H. Gypsum, a tricky material. *Soil Sci. Soc. Am. J.* **2009**, *73*, 1757–1763.
76. Sickels-Taves, L.B.; Allsopp, P.D. Lime and its place in the 21st century: Combining tradition, innovation, and science in building preservation. In Proceedings of the International Building Lime Symposium, Orlando, FL, USA, 9–11 March 2005, p. 14.
77. Cowper, A.D. *Lime and Lime Mortars*; Routledge: Abingdon-on-Thames, UK, 2017; ISBN 9781873394298.
78. Rampazzi, L.; Pozzi, A.; Sansonetti, A.; Toniolo, L.; Giussani, B. A chemometric approach to the characterisation of historical mortars. *Cem. Concr. Res.* **2006**, *36*, 1108–1114.
79. Gómez-Pujol, L.; Roig-Munar, F.X.; Fornós, J.J.; Balaguer, P.; Mateu, J. Provenance-related characteristics of beach sediments around the island of Menorca, Balearic Islands (western Mediterranean). *Geo-Marine Lett.* **2013**, 33, 195–208.
80. La Spina, V.; Mileto, C.; Vegas, F. Characterisation of Roman and Mediaeval renderings. The case of the remains found in archaeological excavations in the city of Valencia (Spain). *J. Archaeol. Sci. Rep.* **2016**, 10, 30–43.
81. Mileto, C.; Vegas, F.; La Spina, V. Is gypsum external rendering possible? The use of gypsum mortar for rendering historic façades of Valencia's city centre. In *Advanced Materials Research*; Trans Tech Publications Ltd.: Bäch, Switzerland, 2011; Volume 250, pp. 1301–1304.
82. La Spina, V.; Fratini, F.; Cantisani, E.; Mileto, C.; Vegas López-Manzanares, F. The ancient gypsum mortars of the historical façades in the city center of Valencia (Spain). *Period. Mineral.* **2013**, *82*, 443–457.
83. Fullana, A.G.; Bestard, D.C.; Arbós, P.B. Els forns de guix en les explotacions mineres històriques de la Serra de na Burguesa (Mallorca). *Boll. Soc. Arqueol. Lul Liana Rev. D'estudis Històrics* **2016**, *72*, 221–247.
84. Bover, P.; Ginard, A.; Crespí, D.; Vicens, D.; Vadell, M.; Serra, J.; Santandreu, G.; Barceló, M.A. Les cavitats de la Serra de na Burguesa. Zona 6: La mineria a la Serra d'en Marill (Palma, Mallorca). *Publicació D'espeleologia* **2004**, *26*, 59–82. Available online: https://raco.cat/index.php/Endins/article/view/122499 [Accessed on 23-December-2021].